CHALMERS
UNIVERSITY OF TECHNOLOGY

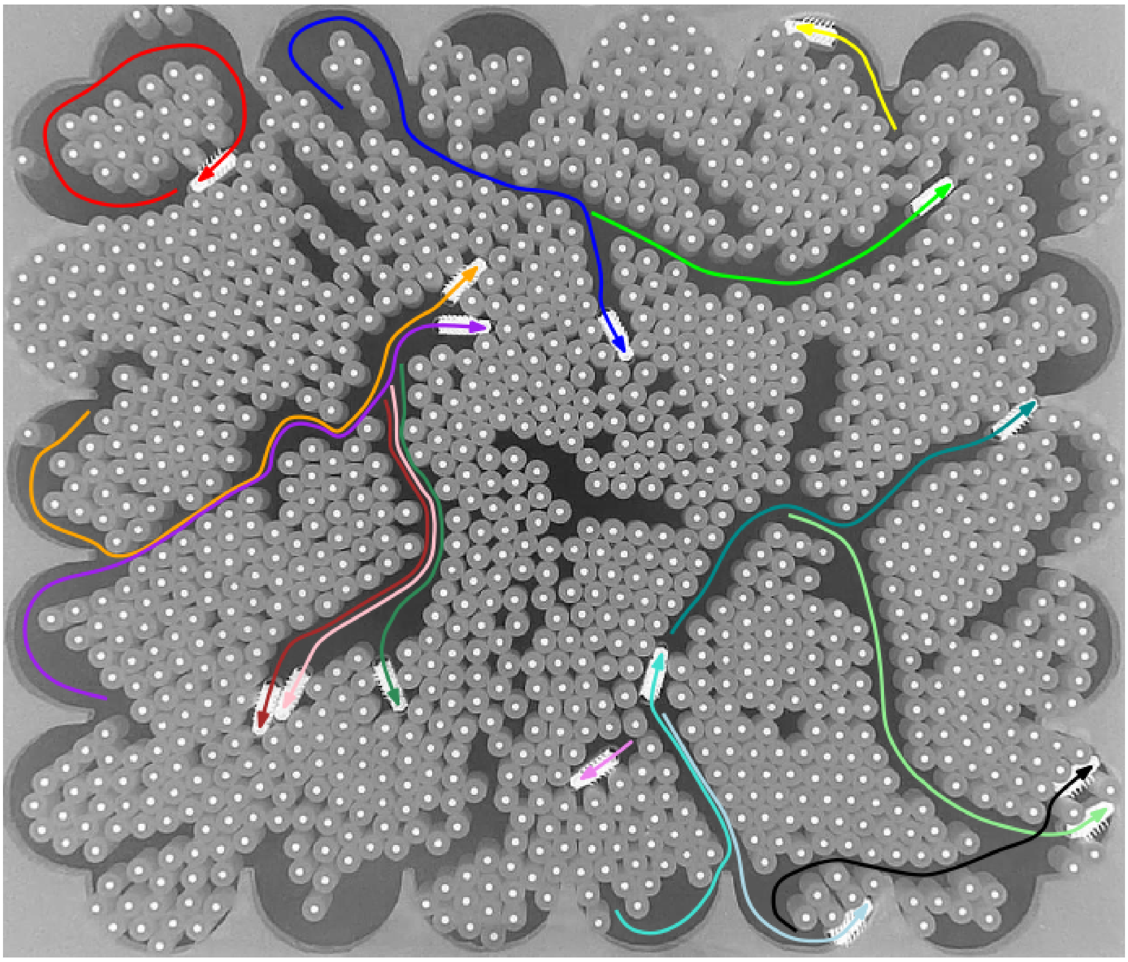

Collective behaviors of autonomous robots in complex environment

A study of emergent behaviors from many simple agents in a complex environment

Master's thesis in Complex Adaptive Systems

THOMAS SUPHONA

Department of Applied Physics
CHALMERS UNIVERSITY OF TECHNOLOGY
Gothenburg, Sweden 2021

Master's thesis 2021:NN

Collective behaviors of autonomous robots in complex environment

A study of emergent behaviors from many simple agents in a complex environment

THOMAS SUPHONA

CHALMERS
UNIVERSITY OF TECHNOLOGY

Department of Applied Physics
Division of Soft matter lab
Soft matter lab
Chalmers University of Technology
Gothenburg, Sweden 2021

Collective behaviors of autonomous robots in complex environment
A study of emergent behaviors from many simple agents in a complex environment
THOMAS SUPHONA

Supervisor: GIOVANNI VOLPE, University of Gothenburg
Examiner: GIOVANNI VOLPE, University of Gothenburg

Master's Thesis 2021:NN
Department of Applied Physics
Soft matter lab
Soft matter lab
Chalmers University of Technology
SE-412 96 Gothenburg
Telephone +46 31 772 1000

Cover: Visualization of trajectories used by robot bugs in an environmment of plastic cylinders.

Typeset in LaTeX
Gothenburg, Sweden 2021

Collective behaviors of autonomous robots in complex environment
A study of emergent behaviors from many simple agents in a complex environment
THOMAS SUPHONA
Department of Applied Physics
Chalmers University of Technology

Abstract

Collective behaviors or collective motion is a common phenomena in nature where multiple organisms in a system undergo ordered movements. This can be observed in different scales, from the microscale with bacteria swarming to the macro scale with for example flocks of birds, schools of fish and even human crowds and car traffic. All these systems are made up by self-propelling agents who are able to take up energy from their environment and converting it to directed motion. Because of this property of self-propulsion, their dynamics cannot be explained using conventional methods. Although significant efforts have been made in trying to explain collective behaviors from different perspective, using simulation tools and study systems in different scales, the subject is not as widely studied from the macroscale, especially with artificially made systems. In this thesis, a macroscale system was designed with the purpose of providing conditions for collective behaviors to emerge and study how the behaviors changes depending on the surrounding conditions. Battery powered robots were used as self-propelling agents and they were placed in a confined space filled with obstacles. It was shown that when the number of robots and obstacles inside the system is large, the robots movements were significantly restricted. The weight of the obstacles do also affect the average motions of the robots where heavier obstacles hinder the robots by creating blockage leading to the robots having lower average velocity. At certain configurations of the parameters, the robots showed collective behaviors where they for example form channels between the obstacles, making "roads" for other robots to reuse, or helping each other to move by pushing away chunks of obstacles or pushing onto each other. Even though these robots are simple agents, they have managed to manifest cooperative actions towards other agents.

Keywords: collective behaviors, complex environment, flocks, swarm.

Acknowledgements

Many people have contributed to this project and first and foremost I would like to give credit to Giovanni Volpe for proposing this project and being my supervisor and examiner. I would also like to thank Alessandro Maguzzú for helping out with many of the practical side of the project, giving good advises and suggestions steering the project in the right direction. This project wouldn't be possible without Filip Dahlsbecker's and Mokhtar Mapar's contribution with their expertise and resources of 3D printing. I am also grateful to Quentin Pikeroen with his assistance and input to the project, both the experimental and the analysis part, and also for putting up with the long experiments. Lastly I would like to thank all the people in Soft Matter Lab for their kindness and encouragement providing a pleasant environment through the course of this thesis.

Thomas Suphona, Gothenburg, June 2021

Contents

1
Introduction

With many particle systems, one of the most interesting aspects is the complex collective behaviors that emerge. In nature, this behavior can be observed in, schools of fish moving as a unit, flocks of birds flying uniformly as group, herd of land animals and even human crowds. These phenomena are fascinating to observe and study, because the mechanisms behind the collective behaviors are far from obvious.

Collective behaviors have been studied in great detail for the last decades. Early on, self-propelled particles were studied to model the swarm behavior of animals at the macroscale[1]. Reynolds introduced in 1987 a "Boids model" to simulate noncolliding aggregate motion, such as that of flocks of birds, heards of land animals, and schools of fish within computer graphics applications[2]. In 1995, Vicsek and co-authors introduced the "Vicsek model" where the swarm behavior is modelled by active particles that are driven with a constant absolute velocity and they tend to align with the average direction of motion of the particles in their neighbourhood[3]. The Vicsek model was the first model to look at collective motion as a noise-induced phase transition. Then later on, several other models have been introduced aiming to study and explain the properties of collective behaviors[4]–[10]. Experimental studies have also been done on systems with complex collective behaviors[11]–[15]. The collective behavior in swarming systems turns out to occur in many different scales, and furthermore the behaviors are robust and universal e.g. the animals share group-level properties, irrespective of the type of animals in the group[16].

With the "Vicsek model", active particles were introduced to model the swarm behavior. The term "active" refers to the ability of the individual particles to move actively by gaining energy from the environment[17]. Examples of such systems range from microsystems such as brownian motors[18] and motile cells[19]–[21], to macroscopic animals[22], [23] and also artificial self-propelled particles[24], [25]. Active particles are able to propel themselves and perform active motion due to an internal driving. This could have been caused by different factors such as biological activity or non-equilibrium dynamics in artificial driven systems[17]. This ability of self-propulsion is a common feature in microorganisms[26]–[28], which allows the organisms for a more efficient way to search for nutrients or avoid toxic substances[29]. In contrast to the active particles, the motion of passive particles is the standard dynamical behavior of particles suspended in a medium, and is driven by equilibrium thermal fluctuations, due to random collisions with the surrounding fluid molecules[30].

Some of the most generic models used to describe active particles systems can be considered as an extension of well known concepts in physics such as Brownian motion. Brownian motion, being purely physical in origin and having a central role in the foundation of thermodynamics and statistical physics, is now a major interdisciplinary research topic. The concept of self-propulsion is often studied in the framework of active Brownian particles. In many publications the term ”Active Brownian Particles” is used to refer to self-propelled particles far from equilibrium (see e.g [31]–[35]). Here, we will refer to ”Active Brownian Particles” as Brownian particles performing active Brownian motion.

In recent years, active Brownian motion has attracted the interest of the biology and physics communities[28], [36]. Several types of microscopic biological systems perform active Brownian motion. Understanding their motion can provide insight into out-of-equilibrium phenomena[37] and lead to the development of novel strategies for designing smart devices and materials[1]. The possibility of designing and using active particles in real world application is immense, ranging from the targeted delivery of drugs, biomarkers, or contrast agents in health care applications[38]–[41], to the autonomous depollution of water and soils, climate changes, or chemical terroristic attacks in sustainability and security applications[42].

Active particles provide great hope in adressing the many challenges of our modern societies and a significant and growing effort has been pushed to advancing this field and to explore its applications in a diverse set of disciplines[1]; in statistical physics[43], biology[29], robotics[44], social transport[45], soft matter[46] and biomedicine[39]. The potential applications can be built around the core functionalities of active Brownian particles, with transport, sensing and manipulation, which can lead to smart designs of nanomachines and micromachines that can perform tasks in an autonomous, targeted and selective way.

This property of universality and scalabilty of collective behavior will be the main focus of this thesis, especially on systems in macroscale. And efforts will be made in trying to answer whether a model describing the behavior of active Brownian particles is scalable i.e. valid in different scales.

1.1 Related works

A study was done in 2017 by Nilsson and Volpe using a simulation of active particles with short-range aligning interactions[47]. This model was studied numerically as a function of orientational noise parameter. The simulation was done with and without the presence of passive particles, and it was shown that, with the presence of passive particles, the active particles transition from a diffusive state, at high noise levels, to a state of which they can propagate unhindered along a network of metastable channels as the noise level is decreased.

In this model, the position $\boldsymbol{x}_n$ and direction θ_n, of particle n is updated each timestep $t = 0, 1, 2, \ldots$ according to

$$\begin{cases} \boldsymbol{x}_n(t+1) & = \boldsymbol{x}_n(t) + \boldsymbol{v}_n(t+1) \\ \theta_n(t+1) & = \theta_n(t) + T_n + \xi \end{cases} \tag{1.1}$$

The particles are hard spheres with a constant speed of $|\boldsymbol{v}_n| \equiv v$, ξ is a white-noise term which is uniformly distributed in the interval $[-\eta/2, \eta/2]$, and T_n is a torque term. The torque term describe the torque exerted on particle n by all other particles, active and passive, and is expressed as follows

$$T_n = T_0 \sum_{i \neq n} \frac{\hat{\boldsymbol{v}}_n \cdot \hat{\boldsymbol{r}}_{ni}}{r_{ni}^2} \hat{\boldsymbol{v}}_n \times \hat{\boldsymbol{r}}_{ni} \cdot \hat{\boldsymbol{e}}_z - T_0 \sum_m \frac{\hat{\boldsymbol{v}}_n \cdot \hat{\boldsymbol{r}}_{nm}}{r_{nm}^2} \hat{\boldsymbol{v}}_n \times \hat{\boldsymbol{r}}_{nm} \cdot \hat{\boldsymbol{e}}_z \text{ for } r_{ni}, r_{nm} < r_c, \tag{1.2}$$

The first term in eq. (1.2) describes the torque exerted on the active particle n by all other active particles. The second term is the torque exerted on the same active particle n by all the passive particles m where $m = 1, \ldots, M$. For more detail on the theory, see [47]. A simulation of this model was done using 20 active particles and 900 passive particles, with various noise level the result is shown in fig. 1.1

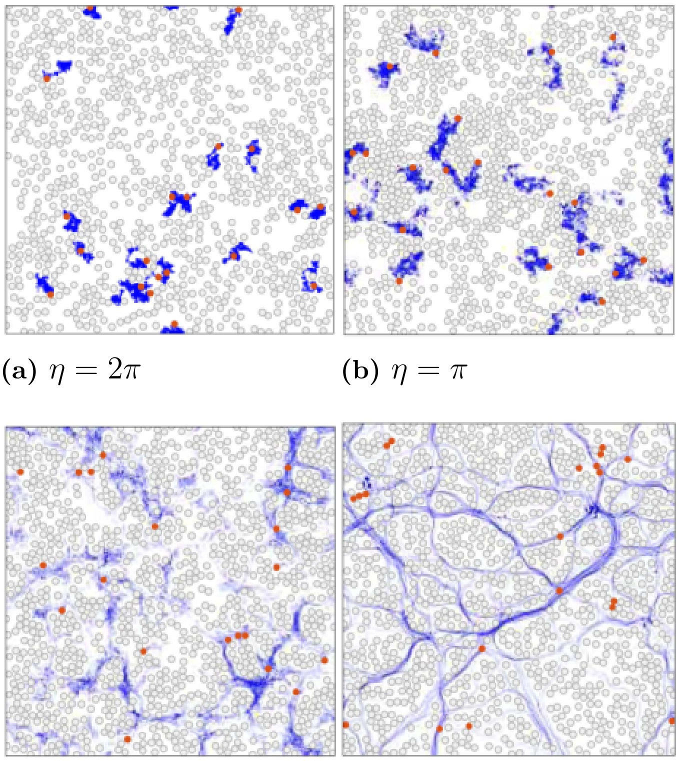

(a) $\eta = 2\pi$ **(b)** $\eta = \pi$

(c) $\eta = 0.5\pi$ **(d)** $\eta = 0.03\pi$

Figure 1.1: Taken from [47], a snapshots at timestep $t = 100\,000$ of a simulation with 20 active particles(red dots) and 900 passive particles(white dots). The behavior of the active particles is captured at 4 different directional noise levels, $\eta = 2\pi$ in **(a)**, $\eta = \pi$ in **(b)**, $\eta = 0.5\pi$ in **(c)** and $\eta = 0.03\pi$ in **(d)**.

At a high noise level with $\eta = 2\pi$ in fig. 1.1a, the active particles motion is significantly restricted and perform essentially a Brownian diffusive motion while being confined in small pockets surrounded by passive particles. On the other hand when the noise level is decreased as in fig. 1.1d, the active particles is able to move freely forming channels to which they can propagate through and resuse.

This behavior was also measured quantitatively in terms of the mean square displacement (MSD), which is a tool to characterise a particles movements, whether a particle spreads randomly due to diffusion, or if there is a force contributing to the movements. The MSD is shown in fig. 1.2.

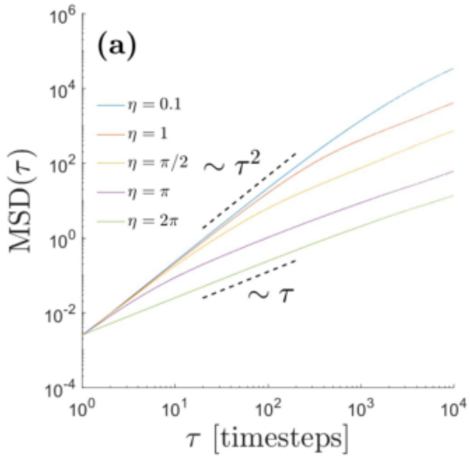

Figure 1.2: From [47] where the MSD of active particles in the presence of passive particles is plotted as a function of the directional noise level (η), in the conditions shown in fig. 1.1.

The MSD shows that at a high noise level where $\eta = 2\pi$, the motion of the active particles is significantly hindered, resulting in the MSD curve having a slope ≤ 1 at all times(green line in fig. 1.2), suggesting diffusion. As the noise level decreases, the MSD becomes ballistic over short times i.e. there is a superdiffusive regime in a small time range where $\text{MSD}(\tau) \propto \tau^2$. The time range of which the MSD is ballistic gets longer as the noise level decreases, and at $\eta = 0.03\pi$ the superdiffusive regime is longest(blue line in fig. 1.2), where there are fully-fledged channels through which the active particles can propagate unhindered, clearly shown by the blue shaded areas, see fig. 1.1d.
This thesis will be largely based on the results from Nilsson and Volpe and the focus will be especially on the dynamics of mixed systems with passive and active particles. We will try to answer whether or not the results above can be reproduced in the macroscale, and also further explore the collective behaviors of the active particles, more specifically the behavior of forming and reusing channels by the active particles.

1.2 Motivation and aim of the thesis

This thesis aims at showing the universality in the collective motions of active particle systems, by studying the behaviors of a system of autonomous agents in a complex environment. It will in particular consider how systems of simple agents can lead to very complex behaviors. More specifically, we want to answer the question whether the result from [47] is universal i.e valid in different scales, and whether or not it is possible to design a system in macroscale to reproduce these results. There are two behaviors in focus that will be investigated in this thesis, first; the phase transition of the active particles from a diffusive state to a ballistic state and second; the channel formation and reusing of channels by the active particles. While this is the main subject of this project, there are efforts being made in parallel within the Soft Matter lab on closely related projects such as experiments with bacterias in a complex environment of obstacles made of glass beads, by Saga Helgadottir, and experiments with Janus particles as active particles with 2.6−lutidine colloids for passive particles, by Giorgio Volpe's and collegues. Being able to compare the results from the different projects with this one will lead to a clearer picture of how systems with active and passive particles behave in different scales and perhaps answer the question whether the behaviors are universal or not. In fact, similar model of active particles have been used in different types of systems of different scales, but it is still a challenge for theoretical physics to find minimal statistical models that can capture these features that are inherent for active particles systems[48]–[50]
The emphasis of studying the autonomous agents in a complex environment is based on the fact that self-propelled particles often move in patterned environments, for example E. coli inside the intestinal tract[51], or chemotactic bacteria moving through porous polluted soils[52]. Thus conducting experiments using complex environment will give a more realistic picture of how real world systems behave.
As pointed out before, the focus is to design and study a system consisting of multiple elements/agents, where each agent is only able to perform simple task as moving forward or turn when hitting an obstacle. The complexity lies in the interaction of these simple agents and their surroundings over time. It will be interesting to study how the system evolves over time and also what factor contributes to a certain behavior.

2

Methods

This thesis is mainly experimental where more emphasis is put on the experiment rather than the theory. The process from start to finish consist of three main parts, the setup, the experiments and the data processing. The bare minimum of what was needed to conduct the experiment was a stage/arena to be the plane of motion, active and passive particles, and a recording contraption for collecting data. Since the scale of this experiment need to more or less resemble the simulation from Nilsson and Volpe, it was clear early on that the arena of motion need to be relatively large, in comparison to the size of the particles. With a large stage, then there was the problem of capturing the whole stage. Also how should the active and passive particles be chosen? These issues will be addressed in the section below.

2.1 The general experimental setup

A opaque glass panel with dimension $113 \times 98\,\mathrm{cm}$ was chosen to be the surface of which the particles will move on. Glass was chosen for the reason that it ensures a hard and smooth surface, also it allows the option of filming the experiment from both above and below. To hold the glass panel tight and steady, a wooden frame was build in a way that allows the glass panel to be easily removed from, and put on to the wood construction. The finished glass table like construction is shown in fig. 2.1

2.2 The boundary frame

Note that fig. 2.1 show the latest iteration of the setup with all its part. In previous iteration the boundary frame which was used for holding the particles inside the arena had a rectangular shape as in the right model of fig. 2.2.

This rectangular shape turn out to be sub-optimal and lead to undesired behaviors with the active particles, where they often align with the walls of the frame and spend most of their time traversing alongside the boundary, see fig. 2.3.

This sort of behavior was undesired since the particles did not interact much with on another and anything related to collective behavior was hard to see. The cloud shaped boundary was made to address this particular issue where the active particles now was redirected back towards center when hitting the wall, see left model in fig. 2.2.

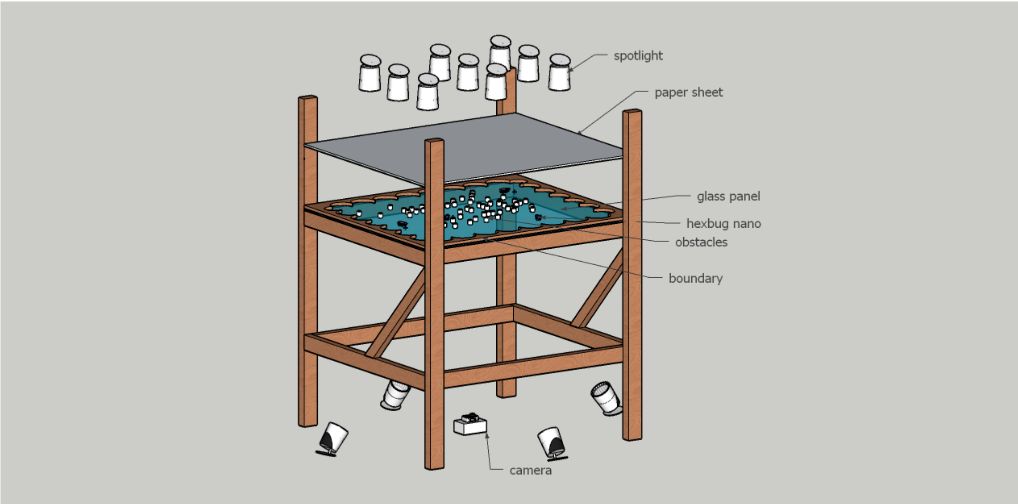

Figure 2.1: A glass table construction where the experiments was conducted on. The construction including the surrounding equipment consist of a main wooden frame with 4 table legs, 13 spotlights, a paper sheet, a glass panel, a boundary frame to prevent the particles from falling from the glass, and a camera centered in the bottom of the table. As an example in this figure, the active and passive particles are placed on the glass labeled as hexbug nano and obstacle, which will be explained shortly.

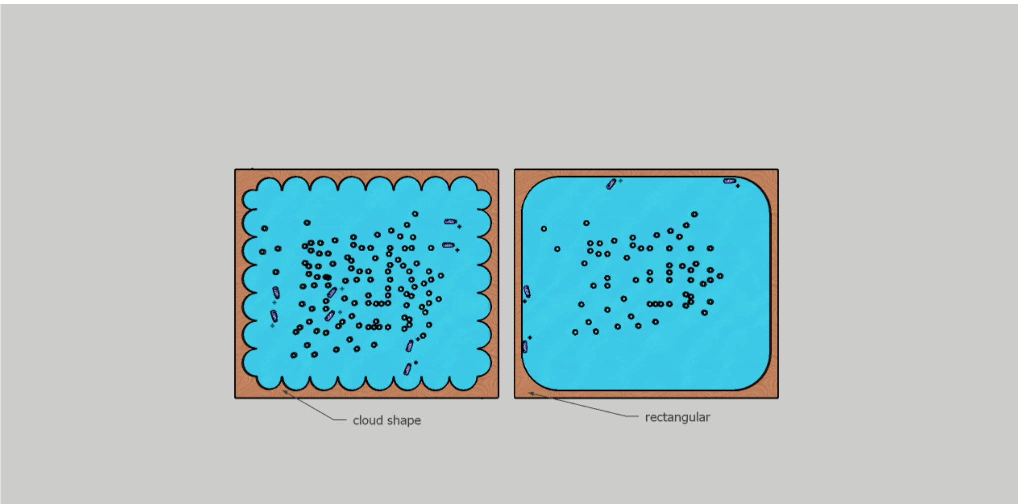

Figure 2.2: The different boundary frame that were used, cloud shaped to the left and rectangular to the right. The cloud shaped boundary(left) is an improvement from the rectangular shaped one(right), with the purpose of redirecting the active particles back to the center.

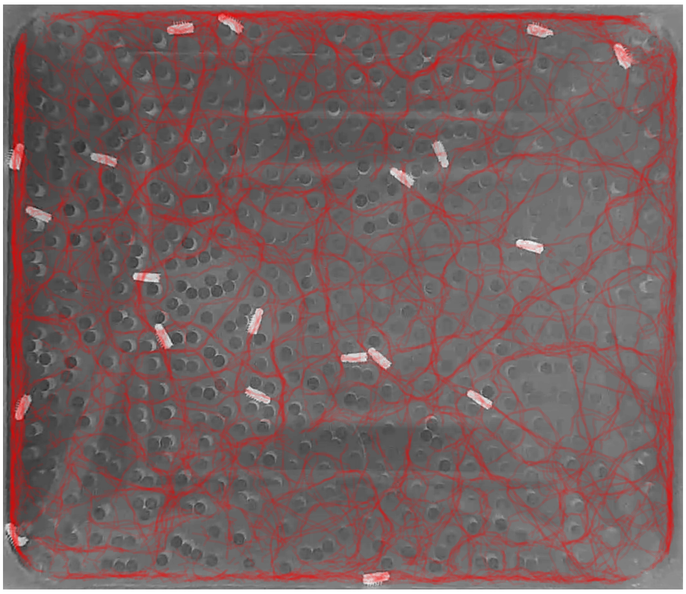

Figure 2.3: A snapshot of an earlier experiment when the rectangular boundary was used. The active particles tend to move alongside the walls of this boundary, as can be seen from their trajectories(red lines) where it is more red at the four edges of the arena, compared to the center.

2.3 The active particles

2.3.1 The original robot bugs

As for active particles in macroscale, toy robots called HEXBUG nano® were used, see fig. 2.4.

Figure 2.4: The commercialized toy robots HEXBUG nano® that were used as active particles in macroscale, they have the dimension $40 \times 15 \times 20$ mm and comes in many different colors, the image is copied from [53].

This is just one of the many products by the company HEXBUG who is specialized in battery powered children's toy. The HEXBUG nano® is a micro robotic creature that uses vibration to propel forward. The vibration is powered by a tiny motor which in combination with the 12 angular legs is able to move the robot forward. The forward movement is a result of the robot legs being slightly bent backward compressing like a spring during the downward motion and then expanding converting elastic potential energy to kinetic energy pushing the robot forward, see fig. 2.5. The directional behavior of the bugs are random, while their velocity depend on the battery power which uses the type cell AG13/LR44 batteries.

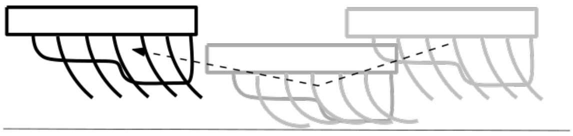

Figure 2.5: A simplified scheme showing how the HEXBUG nano® are able to propel themselves forward using only vibration from a motor and their legs which are tilted backwards.

2.3.2 Solar panel powered bugs

In earlier stage of this project, there was an effort in trying to power the bugs using a solar panel. This was an effort in trying to minimize outside influences to the system, such as changing of batteries, also the intensity of illumination could be used as a parameter where it would affect the bugs activity. The solar panel were placed on top of the bugs using lamps as source of illumination. In the first trial, a different type of commercial toy bug were used. These one was already made with solar panel built in, see fig. 2.6a.

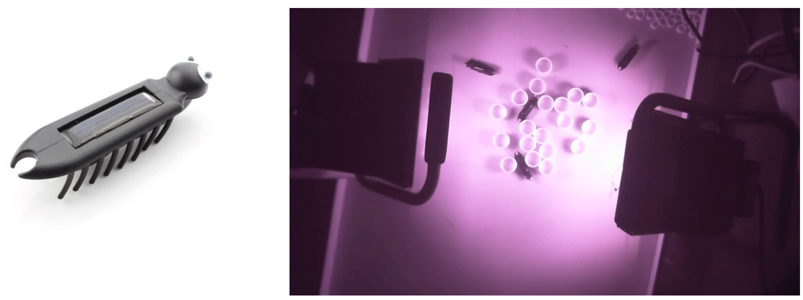

(a) **(b)**

Figure 2.6: Toy solar bugs made in China in **(a)** with dimension $60 \times 15 \times 12\,\mathrm{mm}$, the image is copied from [54]. In **(b)** is an experiment using these bugs with 2 construction spotlights as light source.

These bugs were much less vibrant then the HEXBUG nano and required the light source to be very close to them. Also, they seem to only react on the type of light source that produces a large amount of heat, see fig. 2.6b, which over time does damage on the bugs. Being exposed to heat from lamps, the body of these bugs started to melt and there legs detached from the body as a result from the glue, connecting the legs to the body, melting.
Having the practical issues mentioned above, the solar bugs were replaced with the HEXBUG nano, now with the battery removed and a solar panel mounted on top of the bug, see fig. 2.7.

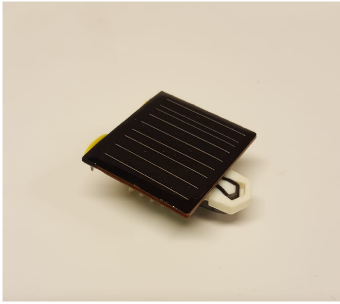

Figure 2.7: The HEXBUG nano® with a solar panel mounted on top. The battery inside the bug was removed and instead there are wires connecting the solar panel to the motor inside.

This arrangement with the solar panel on the HEXBUG, in fig. 2.7 improved the motions of the bugs marginally. The bugs shows more activity compared to the Chinese made ones, but the extra weight and the rectangular geometry of the solar panel created some unwanted behaviors. The extra weight from the solar panel made the bug top heavy which caused them to sometimes tip over, and also if the panel was not centered on the bug well enough, the movement will be biased either left or right. The size of the solar panel with the dimension $35 \times 39\,\mathrm{mm}$ created unwanted contact interactions between the bugs such as the scenario where the solar panels from 2 different bugs would overlap and cling on to each other. With all this being said, the problem of illumination still remains where the illumination is still being too low and inhomogeneous, causing the bugs to move much slower than they would with battery and the speed was rarely constant.
Having all the practical issues mentioned before, the solar powered concept was abandoned and the project proceeded on using the original HEXBUG nano with battery, though with other minor modifications.

2.3.3 The battery powered bugs

As mentioned before, these bugs runs on type cell AG13/LR44 batteries, and can be used up to 4 hours before the battery need to be changed. When letting these bugs run on an empty arena, without passive particles, the bug show some random chirality(a tendency to move to the left or right) resulting in them moving in circles with the radius decreasing over time as the battery gets lower, see fig. 2.8. This chirality is probably a result of some asymmetry with the bug that appears during manufacturing.
This chiral behavior is inherent to the bugs and different bugs has different degrees of chirality which cannot be predicted in beforehand. Though this behavior seems substantial, it can be neglected when the passive particles are introduced where collision-based interactions is dominated and the free running space is minimal.

2.3.4 The shape of the bugs

When using a new fully charged battery on a bug, their activity becomes quite vibrant. This lead sometimes to them tipping up side down ending up on their

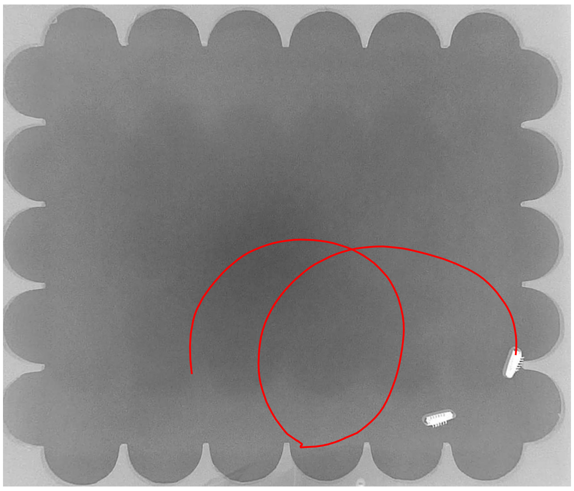

Figure 2.8: An experiment with 2 bugs with only one being tracked with the red line showing its trajectory. The tracked bug was running for approximately six seconds and has almost managed to complete two full circles, which is a result of its chirality.

back or climbing on top of each other. Even the shape of their head caused some unwanted behavior. The pointy shape of their head resulted oftentimes in them being blocked between heavy obstacles, trying to push for a long time instead of finding a new path in other directions, see fig. 2.9.

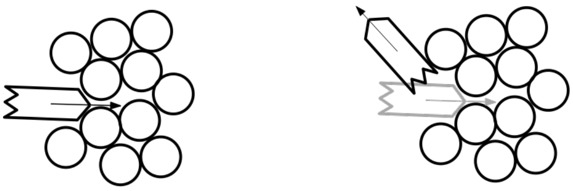

Figure 2.9: To the left is an example scenario where the robot bug is trying to push through heavy obstacles, for a long time instead of finding a new path. To the right is the desired behavior where the bug first tries to push through the obstacles but is unable to, it then changes its direction and finds new path.

The behavior of pushing through obstacles was not entirely unwanted since it was still necessary for the bugs to create channels by pushing the obstacles. However, with the pointy heads, they tend to spend the majority of their time pushing i.e creating channels instead of reusing them, which makes it hard to observe any phase transitions or the reusing of channels.
Two new modifications were made to address this problem, see fig. 2.10.
The first attempt was to glue a piece of plastic circle on the bugs head as in fig. 2.10a, this way the bugs would have a better chance of bouncing away from the obstacles instead of spending too much time trying to push through them. However when using many bugs there was a problem of the circle head overlapping each other and become stuck, upon a collision. These unpredictable behavior required further improvements resulting in the latest version seen in fig. 2.10b.

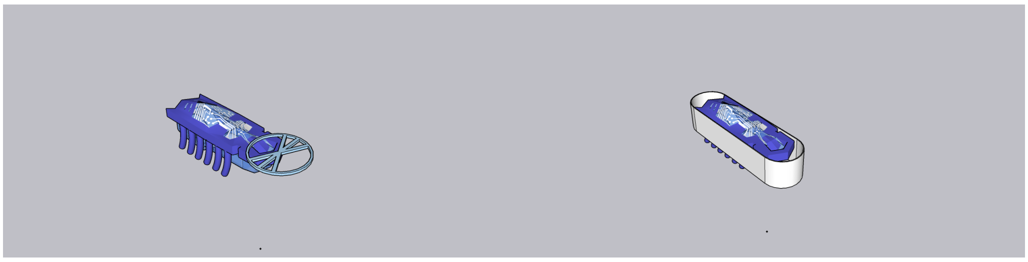

(a) (b)

Figure 2.10: Modified versions of HEXBUG nano, 3D printed plastic circle on the head in **(a)**, and strip of paper wrapped around its body in **(b)**.

This modification here was rather simple using only a strip of paper to wrap around the bugs body. Compared to the previous versions, this modification does not add any significant weight to the original bug since the weight of the paper strip is neglectable compared to the weight of the bug. Also the weight is evenly distributed around the bug which will not amplify the bugs inherent chirality further. This rod shape is quite common in the field of active matter, presenting in theoretical models[55], Janus particles[24], and bacterias[51], and furthermore the rod shape creates aligning interactions, see fig. 2.11, which is advantageous for the emergence of collective behaviors.

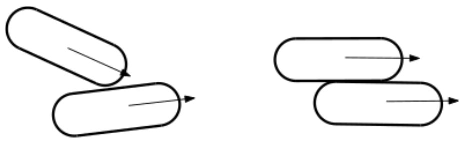

Figure 2.11: An example of aligning interactions between two rod shaped bugs upon collision.

With all the advantages mentioned, only the rod shaped bugs will be used to produce the results presented in this thesis. For future reference, the terms active particles, robot bugs or bugs will be used interchangeably, referring to the Hexbug nano wrapped in paper strip.

2.4 The passive particles

The passive particles that were use to make up the complex environment are 3D printed plastic cylinder see fig. 2.12. These cups are approximately 19.5 mm in diameter, 20 mm in height and weighs 2 g.
To vary the weight of each cylinder, M8 nuts were used to be placed inside the cylinders. The nuts weigh 5 g each, and each cylinder can hold up to three nuts. The possible weight that one cylinder can have is 2 g(empty), 7 g(1 nut), 12 g(2 nuts) and 17 g(3 nuts). From this point on, for the sake of clarity, the term obstacle and passive particle will be used interchangeably.

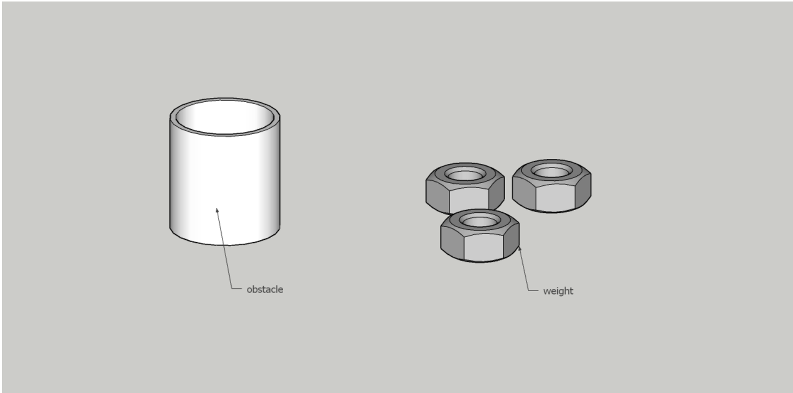

Figure 2.12: 3D printed plastic cylinders(left) used as macroscale passive particles, made hollow in the middle for the purpose of varying its weight by putting M8 nuts(right) in them. The cylinder have dimensions 19.5×20 mm(radius $\times$ height) and weigh 2 g each. The M8 nuts weigh 5 g each and only 3 nuts can be put in one cylinder.

2.5 To record the experiments

The equipment used to record the experiments is the wide angle Victure action camera AC200[56], see fig. 2.13.

Figure 2.13: The wide angle action camera Victure AC200 that was used to record the experiments. This image is copied from [57].

The choice of this particular type of camera was that a regular camera wouldn't be able to capture the entire stage of 88.5×75.4 cm. The ability of filming in a wide angle, which is a common feature in many action cameras, made it possible to capture the entire stage. The camera, being small and compact, made it fairly easy and practical to handle, especially in situations where it is needed to be removed or adjusted.
The setup for the camera is shown in fig. 2.1 where the camera is placed on the ground directly under the table. The camera needed to be fixed still at the center of the table to avoid any distortion to the footage.
When one of the first experiments were filmed, it was clear that the lighting condition was an issue. The source of illumination then, was halogen lamps on the ceiling of the room which decreased the quality of the images significantly, see fig. 2.14.

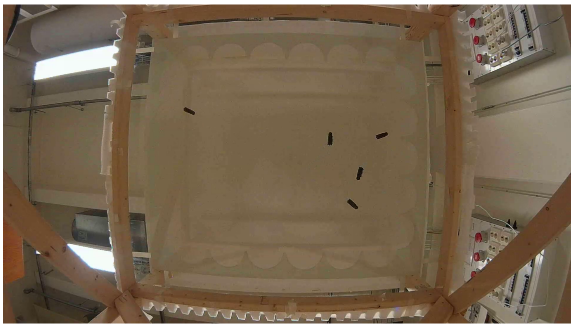

Figure 2.14: Low quality image as a result of bad lighting condition. Reflection of the bottom part of the wood construction can be seen on the glass panel.

To improve the quality of the footage, the lighting needed to be changed. Many configurations were tried out with changing the source of illumination, their placement and from which angle they should illuminate from. The final configuration found that gave the optimal lighting condition is shown in fig. 2.1. This setup consist of 4 spotlights placed on the floor illuminating the glass panel from 4 sides at a 45° angle, and 9 spotlights above the table in an 3 by 3 array illuminating directly down on the paper sheet on top of the table. With this arrangement the quality and contrast of the image improved significantly. The result of this improved lighting arrangement is show in fig. 2.15a, and a photograph of the lab is shown in fig. 2.15b. Additional attempt were made in trying increase the contrast of bugs and obstacles against the white background, where the bugs body were painted black and black dots made of paper were glued under the obstacles.

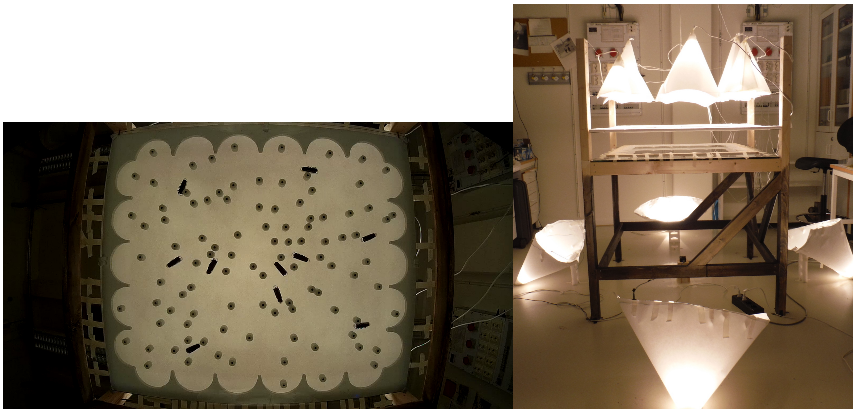

(a) **(b)**

Figure 2.15: In **(a)** an image taken with the improved lighting condition, with better quality and contrast. The overview of the setup inside the lab with improved lighting is shown in **(b)**.

2.6 The Experiment

2.6.1 How to design an experiment

The aim of this thesis is to design a system in macroscale, consisting of active and passive particles, that is able to undergo a phase transition similar to the result from [47]. The system should also show, at some condition, the behavior where the active particles form channels and reusing them. In the simulation from [47], the collective behavior of the active particles changes with a noise parameter, where the active particles at a high noise level could not move far from its starting point, and with lower noise level they could move unhindered and forming channels in an environment of passive particles.
Since with our robots, there is no obvious way to introduce a similar noise parameter. To recreate a similar conditions, we instead use the weight of the obstacles as a "noise parameter" where the heavier obstacles corresponds to the case of high noise in the simulation and lower weight obstacles corresponds low noise in the simulation. The number of obstacles and the number of bugs were also used as parameters. One could already guess that a setting with low obstacle density and low obstacle weight will lead to the bugs undergoing super-diffusive motion(moving with constant speed). To the opposite, having high obstacle density and high obstacle weight will lead to sub-diffusive motion with the active particles since their motion will be significantly impeded by the heavy obstacles. The different variations of number of bugs B, number of obstacles C with W nuts inside, are as follows

$$
\begin{aligned}
B &= \{1, 2, 5, 10, 15, 20, 25\} \\
C &= \{100, 200, 300, 400, 500, 600, 700, 800, 900, 1000, 1100, 1200, 1300\} \\
W &= \{0, 1, 2, 3\}
\end{aligned}
$$

Note that W is a variable showing the number of nuts being used in each obstacles. The weight of a M8 nut is $m_{\text{nut}} = 5\,\text{g}$ and the weight of an empty cylinder is $m_{\text{cyl}} = 2\,\text{g}$. The weight of an obstacle or passive particle can then be expressed as

$$m_{\text{passive}} = W(i) \cdot m_{\text{nut}} + m_{\text{cyl}}$$

which be eigther $2\,\text{g}$, $7\,\text{g}$, $12\,\text{g}$ or $17\,\text{g}$. The number of experiments N_{exp} that was conducted can be calculated as

$$
\begin{aligned}
N_{\text{exp}} &= n(B) \times n(C) \times n(W) \\
&= 364
\end{aligned}
$$

where $n(B)$, $n(C)$ and $n(W)$ are the length of the vectors B, C and W.
In addition to these, experiments without obstacles were made using 1, 2, 5, 11, 16 and 21 bugs, which is 6 additional experiments. This gives the total number of experiments that were made to 370.

2.6.2 Conducting the experiments

One experiment corresponds to a roughly 3 min video with a chosen number of bugs, obstacles and weight of the obstacles. The procedure of conducting the experiment as efficient as possible goes as follows

1. **Preparation**
   1.1. Put on the the glasspanel the chosen number of obstacles and weights and spread them out as randomly as possible.
   1.2. Check if the batteries of the 25 bugs are good, meaning that they are not going to run out after some minutes. If the batteries are to low, change it and make sure to have spare bugs with enough battery power in case a bug run out of battery during an experiment.
   1.3. Take a picture of the stage with obstacles on it and use the MATLAB program `testDetection.m` to track the obstacles and see if the number is as expected.
2. **Execution**
   2.1. When the preparations are done, turn on the camera and start filming.
   2.2. Put the first bug on the stage and let it run from time 0−3 min.
   2.3. Put the second bug on the stage and let it run from time 3−6 min.
   2.4. Put three more bugs on the stage at time 6 min and let in total 5 bugs run from time 6:30−9:30 min. The reason for letting them run from 6:30 min instead of 6 min is to have a time gap for checking if any bugs run out of batteries and that the stage looks ok. If there is anything to be fixed, it should be done before time 6:30 min.
   2.5. Put five more bugs on the stage at time 9:30 min and let in total 10 bugs run from time 10:00−13:00.
   2.6. Put five more bugs on the stage at time 13:00 min and let in total 15 bugs run from time 13:30−16:30 min.
   2.7. Put five more bugs on the stage at time 16:30 min and let in total 20 bugs run from time 17:00−20:00 min.
   2.8. At last put five more bugs on the stage at time 20:00 min and let in total 25 bugs run from time 20:30−23:30 min.
   2.9. One single video file of roughly 24 min long contains 7 experiments where the number of bugs varies. When changing the number of obstacles and the weight, the same procedure above is followed.
3. **Postprocess**
   3.1. As mentioned above one video file contains 7 experiments. Where the number of bugs are varied. So to separate the different experiments, the 24 min video is cut and the part containing a specific number of bugs is saved as separate video files. During cutting of the videos it is important to remove parts of the footage that contains unwanted disturbances such as shadows or hands of the experimenter, which should be removed from the footage.
   3.2. When the videos are cutted, they need to be undistorted since the camera has a fish eye distortion. To achieve this, a MATLAB program was written to converting the distorted video footage to image sequences where one image corresponds to one frame of the video.

3.3. After undistortion, the image sequences are binarized, meaning changing the image sequences to black and white. This is for the purpose of increasing the contrast between the objects that need to be tracked and the background.

3.4. When the image sequences are binarized they are tracked using two different sets of codes, one for tracking the obstacles and one the bugs.

The process of proceeding through the above steps for all the 370 experiments took quite some time. When all the steps were done, the data was save as Matlab structures holding information of the particles trajectories, orientation, also the setting of the experiment with the number of bugs, number of obstacles and the weight of the obstacles.

3

Results

3.1 Mean Square Displacement

The main objective that was mentioned before is to try to observe how the behavior of the particles change with the parameters being used, the number of bugs, the number of passive particles and the weight of the passive particles. More specifically if any phase transition similar to [47] can be observed. A good way to start is to use the same quantitative measurement to see if there are any similarities. Firstly, the mean square displacement (MSD) of the active particles is measured. Using MSD will give us an idea about the character of the active particles motion over time. The MSD is often used to check whether the motion of a system is due to diffusion or if there is a force contributing. The mean square displacement in 2-dimensions can be expressed as follows

$$\begin{aligned} MSD(\tau) &= \langle (x(t+\tau) - x(t))^2 + (y(t+\tau) - y(t))^2 \rangle && (3.1) \\ &= \frac{1}{N-\tau} \sum_{t=1}^{N} (x(\tau+t) - x(t))^2 + (y(\tau+t) - y(t))^2 && (3.2) \end{aligned}$$

What is to be expected is the result from [47] where the MSD for the active particles is higher at a low noise level, in our case low obstacle weight, and the MSD lower at a high noise level, high obstacle weight in our case. Other expected results from the experiment are also that MSD will be higher for cases with low obstacle density.
Firstly the active particles MSD is measured as a function of number of bugs. In fig. 3.1 the MSD of the active particles is calculated in 4 cases with different obstacle weights.
A general trend can be observed from fig. 3.1 where the MSD is lower when the number of active particles is high, and inversely the MSD is higher when the number of active particles is low.
How the number of active particles affect the MSD is not obvious, compared to the obstacle weight as a parameter where there is a strong intuition of the fact that heavier obstacles will prevent the bugs from moving, hence lower MSD. There are though certain behaviors from the active particles that depend on their number and might in turn affect the MSD. This will be discussed further in section 3.3

For the case of varying the weight of the obstacles, the result is shown in fig. 3.2. This shows that while keeping the number of obstacles and number of bugs fixed, the MSD is lower for the cases with high obstacle weight, this result was expected

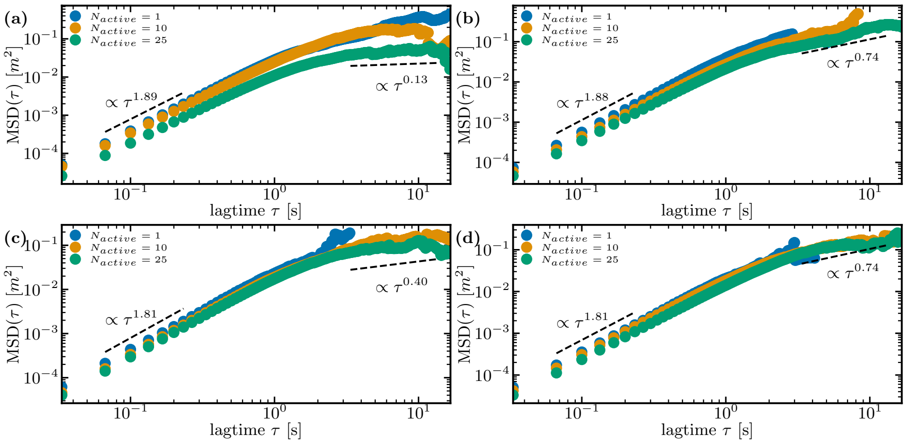

Figure 3.1: MSD for the active particles in 4 different experiments where the number of active particles is used as a parameter. As can be seen, the MSD is slightly lower when the number of active particles is high and this trend holds for different obstacle weights, which is shown in **(a)** with $m_{\text{passive}} = 2 \times 10^{-3}\,\text{kg}$, **(b)** $m_{\text{passive}} = 7 \times 10^{-3}\,\text{kg}$, **(c)** $m_{\text{passive}} = 12 \times 10^{-3}\,\text{kg}$, and **(d)** $m_{\text{passive}} = 17 \times 10^{-3}\,\text{kg}$.

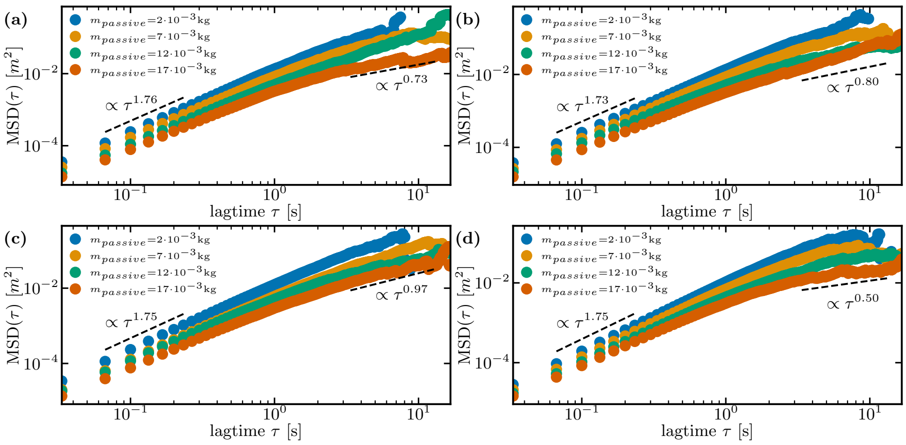

Figure 3.2: MSD for the active particles as a function of obstacle weight. An expected result where the MSD is lower when the obstacle weight is high. Since it is harder for the active particles to push heavy obstacles, they will then move less and this will lead to them having lower MSD. This same trend can be observed with different number of active particles with $N_{\text{active}} = 10$ in **(a)**, $N_{\text{active}} = 15$ in **(b)**, $N_{\text{active}} = 20$ in **(c)** and $N_{\text{active}} = 25$ in **(d)**.

since it is harder for the bugs to push heavier obstacles which will resulting in them having lower speed throughout the experiment. The weight of the obstacles is a parameter that is suppose to mimic the orientational noise parameter in [47] and to compare the result from this paper we can see in fig. 1.2 that the curves is higher for the cases with low noise level (η), similar with the experimental result in fig. 3.2. In the simulation from Nilsson and Volpe, the active particles MSD transition from a superdiffusive motion at small times (MSD $\propto \tau^{\alpha}$, $\alpha > 1$ for small τ), to diffusive motion at long times (MSD $\propto \tau^{\alpha}$, $\alpha \leq 1$ for large τ). This similar behavior can also be observed in the experiment in fig. 3.2 where, for small times the exponent $\alpha > 1$ which suggest superdiffusion and $\alpha \leq 1$ for large times suggesting diffusiv motions. For the last case of studying MSD as a function of obstacles density, the result is shown in fig. 3.3.

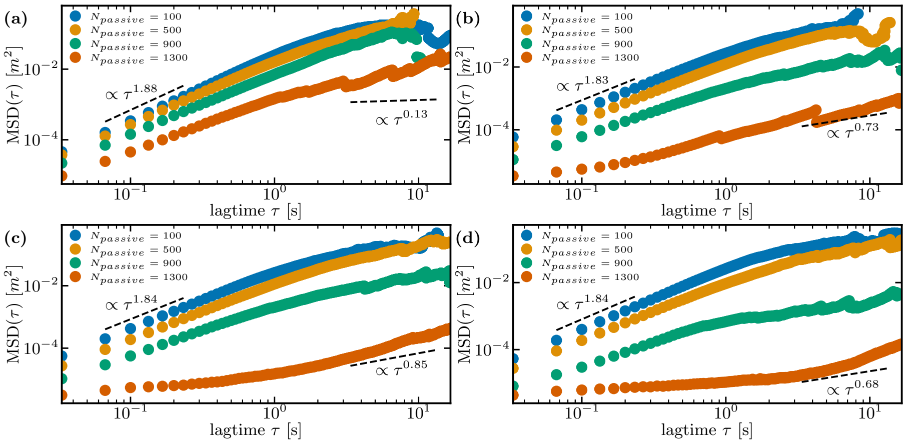

Figure 3.3: Here varying the obstacle density the MSD decreases when the obstacle density increases. Another expected result where the active particles have lesser space to move when the arena is filled with more obstacles. When the arena is packed with the number of obstacles as high as 1000-1300 obstacles, the active particles will be significantly hindered and unable to move from their starting position, this leads to them having MSD close to zero throughout time τ. The different figures show MSD as a function of obstacle density at different obstacle weight, with $m_{\text{passive}} = 2 \times 10^{-3}$ kg in **(a)**, $m_{\text{passive}} = 7 \times 10^{-3}$ kg in **(b)**, $m_{\text{passive}} = 12 \times 10^{-3}$ kg in **(c)**, and $m_{\text{passive}} = 17 \times 10^{-3}$ kg in **(d)**.

Here calculating the MSD of the active particles as a function of the obstacle density, it shows that the MSD is higher for the cases with low obstacle density and decreases as we increase the number of obstacles in the experiment. An expected result where less space is available for the active particles to move freely as the number of obstacles increases and particle-to-obstacle collisions is more frequent.

3.2 Velocity

To study how the weight of the obstacles affect the behavior of the active particles, it is desirable to maximize the interactions between the bugs and the obstacles. To achieve this, the experiment with 1200 obstacles and 25 bugs was chosen. The result of how the active particles velocity get affected by the weight of the obstacles is shown in fig. 3.4.

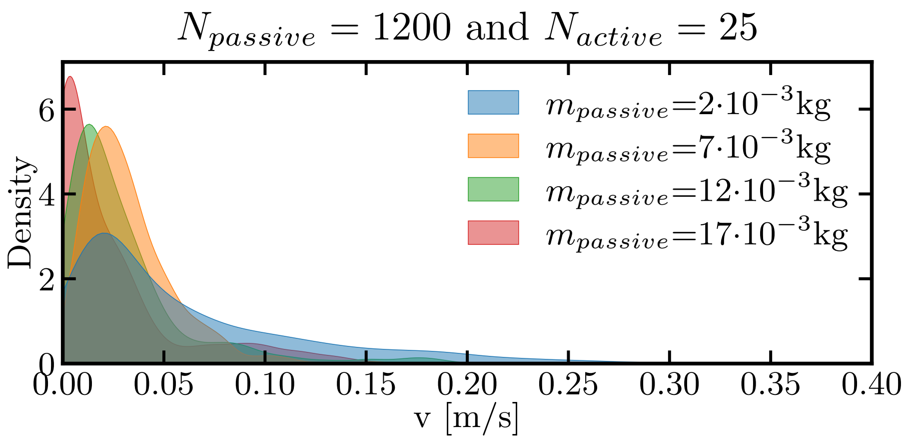

Figure 3.4: Probability distribution of the active particles velocity depending on the obstacle weight. All the four cases were done using 25 active particles and 1200 obstacles, while the different obstacle weight cases has their probability distribution peaks at velocity close to zero, the distribution for lower obstacles weight has lower peak, slightly shifted to the right and also has a fatter tail. Compare for example $m_{\text{passive}} = 2 \times 10^{-3}\,\text{kg}$(blue) and $m_{\text{passive}} = 17 \times 10^{-3}\,\text{kg}$(red).

Here all the cases were done using 25 active particles and with 1200 obstacles, while the weight of the obstacles varies in 4 cases, $m_{\text{passive}} = 2 \times 10^{-3}\,\text{kg}$, $m_{\text{passive}} = 7 \times 10^{-3}\,\text{kg}$, $m_{\text{passive}} = 12 \times 10^{-3}\,\text{kg}$ and $m_{\text{passive}} = 17 \times 10^{-3}\,\text{kg}$ producing the four different probability distribution.
What can be observed in fig. 3.4 is that in all the cases, the probability distributions have similar shapes, peaking around $v \approx 0\,\text{m}\,\text{s}^{-1}$ and decrease as the velocity goes higher. Even though the similar shape of these distributions, one could see that at $v \approx 0\,\text{m}\,\text{s}^{-1}$, the peak of the distribution for lower obstacle weight is slightly lesser than the peak of higher obstacle weight. This result suggest that with a high obstacle density($N_{\text{passive}} = 1200$), regardless of the obstacle weight, the velocity of the active particles will tend to be close to zero. However the probability of active particle having zero velocity is highest when using the heaviest obstacle, and as the obstacle weight decreases the bugs probability of having $v > 0\,\text{m}\,\text{s}^{-1}$ increases, according to the distributions in fig. 3.4.
One of the possible explanation of the similar distribution shapes, even though with different obstacle weights, is that when the arena is packed with this many obstacles, close to its maximum packing density, the obstacles have less freedom to move when being pushed by the active particles. This leaves the active particles no options to move, neither by forming a channel nor changing direction to find a new path, leading to them being significantly slowed down or getting blocked by the obstacles, similar to a car in a traffic jam. Also the number of active particles, in these cases 25, may give rise to the situation of overcrowdedness where the active particles work against each other by blocking one another or closing already formed channels and thus preventing movements. With this high packing density and high number

of active particles, regardless of the weight of the obstacles, the movement of the active particles will be minimal which leads to velocity close to zero.
Even though the arena hasn't yet reached its maximum capacity in how many obstacles that can be fit in, with a high obstacle density such as 1200 obstacles, the steady state behavior will be similar regardless of the obstacle weight, which is the active particles being hindered by the obstacles. However, in shorter time periods for example 10 to 20 seconds, there are noticeable differences between the cases of different obstacle weight, as shown in fig. 3.5.

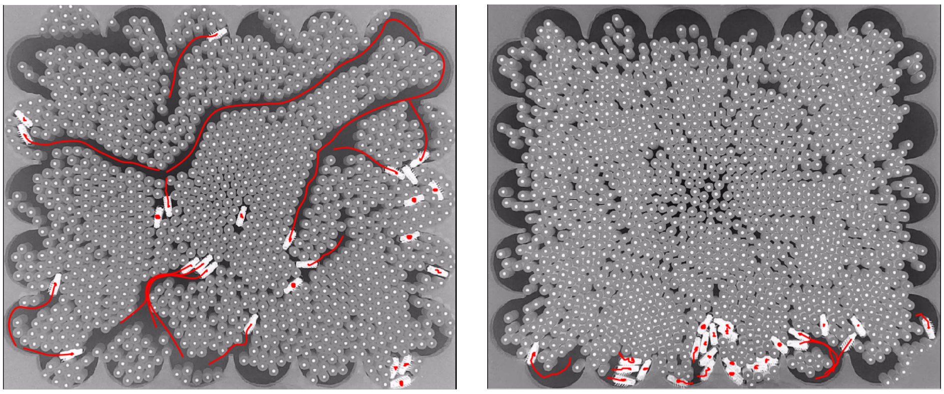

(a) $m_{\text{passive}} = 2 \times 10^{-3}\,\text{kg}$ **(b)** $m_{\text{passive}} = 17 \times 10^{-3}\,\text{kg}$

Figure 3.5: Snapshot of two experiments both at 20 s. Both experiments was done using 25 active particles and with 1300 obstacles wherein **(a)** the obstacle weigh is $m_{\text{passive}} = 2 \times 10^{-3}\,\text{kg}$ each, and in **(b)** $m_{\text{passive}} = 17 \times 10^{-3}\,\text{kg}$ each. The trajectories of the active particles in red lines shows that at the begining in **(a)**, the active particles were able to form and/or reuse channels for a short time, while in **(b)** the active particles remain more or less confined in the same region from where they started.

Seeing the two cases side-by-side one can notice the obvious differences where the case in fig. 3.5a, after letting the active particles run for 20 s they've manage to move the obstacles aside and form some noticeable channels. This activity of forming channels and moving through them last for some seconds and afterwards the majority of the active particles will return to being hindered again, either by pushing a large block of obstacles or by blocking each other and preventing movements.
In fig. 3.5b the active particles will immediately be hindered by the heavy obstacles right from the start, and will spend almost all of their time standing still from being blocked and confined by the obstacles. from pushing the heavy obstacles of $17 \times 10^{-3}\,\text{kg}$ each, leaving all of them with velocities close to zero.
Having seen the results above, one would wonder what happens when the packing density and the number bugs is lower, will there be more noticeable differences between the different obstacle weight? Below in fig. 3.6 shows probability distributions of 4 different packing densities with 100, 400, 700, 1000 obstacles.
The clearest case that shows how the weight of the obstacles affect the velocities of the active particles is the case of 700 obstacles in fig. 3.6**(c)**. Here the distribution shift to the left and gets narrower as the obstacle weight increases, with

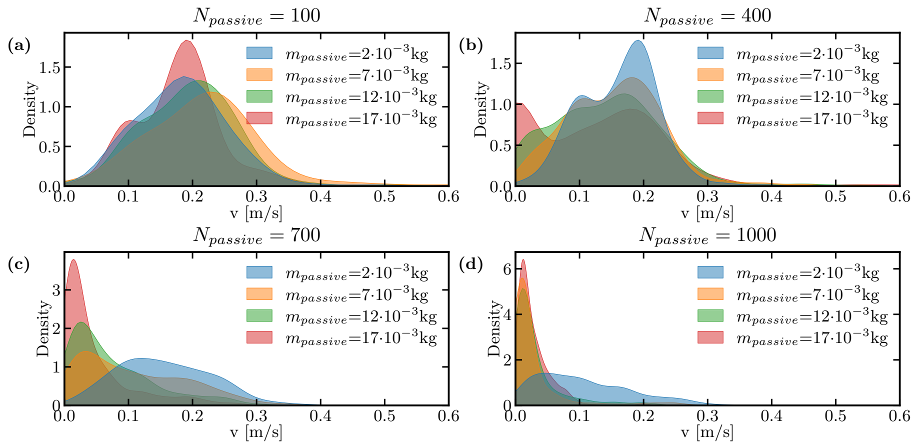

Figure 3.6: Probability distributions of the active particles velocity at 4 different obstacle density. Each figure has 4 distributions corresponding to the different obstacle weight while the number of active particles is fixed to 10. At a high obstacle density case in **(d)**, the probability $p(v > 0)$ for heavier obstacle cases (red, green and orange) is close to zero. The lightest obstacle weight case in blue has its distribution peak significantly lower than the other cases and with a fatter tail, this suggest the situation shown fig. 3.5 where the active particle are able to move more at this obstacle weight. In **(c)** show clearly how the different obstacle weight affect the active particles velocity where, the distribution becomes narrower and shift towards zero velocity as the obstacles becomes heavier.

17×10^{-3} kg(red) having highest peak at $v \approx 0\,\mathrm{m\,s^{-1}}$, followed by 12×10^{-3} kg(green), 7×10^{-3} kg(orange) and 2×10^{-3} kg(blue). This result show how the active particles is being slowed down depending on the obstacle weight, where their velocity is lower in an environment of heavier obstacles.
At lower obstacle densities cases in fig. 3.6**(a)** and **(b)** the range of allowed velocities that the bugs can take seems to be larger i.e. there is nonzero probability for higher velocity, and there is high probability around $v \approx 0.2\,\mathrm{m\,s^{-1}}$. For these cases (fig. 3.6**(a)** and **(b)**) the overall qualitative behavior of the active particles is barely affected by the different obstacle weights, since the interactions between the passive- and active particles are minimal when the packing density is low.
So an observation that can be made from the results in fig. 3.6 is that when the packing density is too low, there is no clear pattern of how the different obstacle weights effect the velocities of the active particles. The threshold of "too low" packing density is found to be about less than 500 obstacles. On the other hand, when having high packing density where $N_{\text{passive}} \gg N_{\text{active}}$, the different obstacle weights doesn't have a significant effect on the active particles, since at a high packing density, e.g. more than 1200 obstacles, regardless of the obstacle weight, the movement of the active particles will be minimal leaving their average velocity close to zero, as shown in fig. 3.7
As can be seen in fig. 3.7**(a)** the active particles average velocity decreases as the number of obstacles increases. How fast this velocity decreases does depend on the obstacles weight where heavier obstacles leads to fastest decrease in velocity, see fig. 3.7**(a)**. At a high packing density at about 1200 obstacles and higher, the

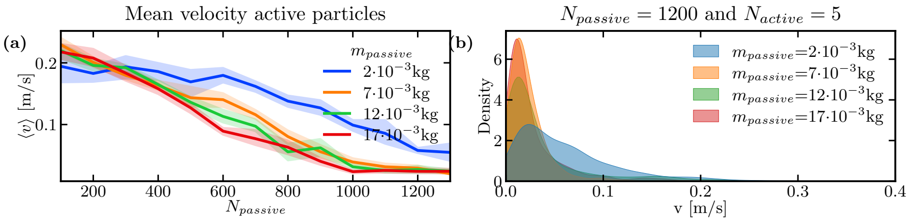

Figure 3.7: To the left in **(a)**, the average velocity of the active particles as a function of the obstacle density shows how the average velocity of the active particles decreases as the number of obstacle increases. The different line correspond to different obstacle weight. The average velocity decreases fastest for the heavier obstacles and the lines for $m_{\text{passive}} = 17 \times 10^{-3}$ kg(red), $m_{\text{passive}} = 12 \times 10^{-3}$ kg(green), $m_{\text{passive}} = 7 \times 10^{-3}$ kg(orange) converges at 1200 obstacles, while $m_{\text{passive}} = 2 \times 10^{-3}$ kg(blue) stays at a higher average velocity. The fact that the blue line doesn't converge with the other lines can also be visualized in **(b)** where the lightest obstacle case(blue) has its distribution peak much lower and also has a fatter tail, at this high packing density.

lines corresponding to the three heaviest obstacle weights, red, green and orange, converges at the same low velocity. The blue line corresponding to the lightest obstacle weight stays at a higher velocity which suggest the scenario mentioned in fig. 3.5 where the active particles, at this light obstacle weight of $m_{\text{passive}} = 2 \times 10^{-3}$ kg, are able to form small channels and move through them for a short period of time, eventhough the packing density is as high as 1200 obstacles.
Previously, the results show that when having the number of active particles fixed, the mean velocity for these active particles decrease towards zero as the number of obstacles increases. As for the weight of the obstacles as a parameter, the mean velocity of the active particles is higher at a low obstacle weight and the velocity is lower when the obstacle weight is high.
A question that needs to be answered is how does the number of active particles affect their mean velocity? Lets answer this by looking at the case where the obstacle weight is $m_{\text{passive}} = 7 \times 10^{-3}$ kg, as shown in fig. 3.8.

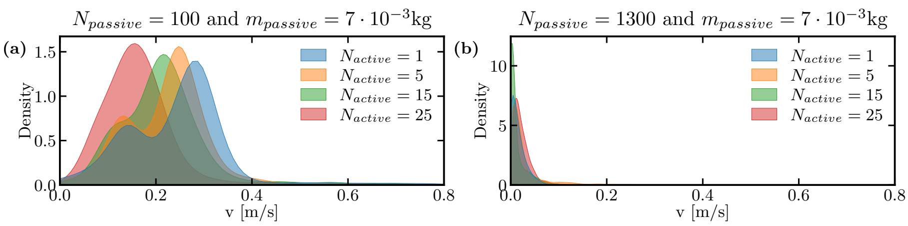

Figure 3.8: Probability distributions of the active particles velocity at two different obstacle density. At low obstacle density in **(a)** the distribution peaks at a lower velocity for the higher number of bugs, while at high obstacle density in **(b)** all the different distribution peaks at a low velocity close to zero.

As pointed out earlier, the active particles velocity decreases as the number of obstacles increases. This again can be seen in fig. 3.8 where the peaks of the veloc-

ity distributions shifts towards $v = 0$ as the number of obstacles increases from $N_{\text{passive}} = 100$, in fig. 3.8**(a)**, to $N_{\text{passive}} = 1300$, in fig. 3.8**(b)**.
When having a closer look at how the number of active particles is affecting the behavior, such as the case with low obstacle density in fig. 3.8**(a)** with $N_{\text{passive}} = 100$, there is a clear separation between the different velocity distributions where the distribution for higher number of active particles peaks at a lower velocity(red), and the distributions shifts towards higher velocity as the number of active particles decreases(blue). This result shows that the probability of having a lower ensemble velocity is higher when the number of active particles is high.
This suggest some sort of crowdedness where the large amount of active particles hinders each other from moving by creating some sort of congestion, see an example in fig. 3.9. As the number of obstacles increases further as in fig. 3.8**(b)**, all the distributions peaks at a velocity close to zero, regardless of the number of active particles. Similar to this result has been seen before in fig. 3.7 where the velocities of the active particles converge towards zero, independent of the obstacle weight, as the packing density increases.

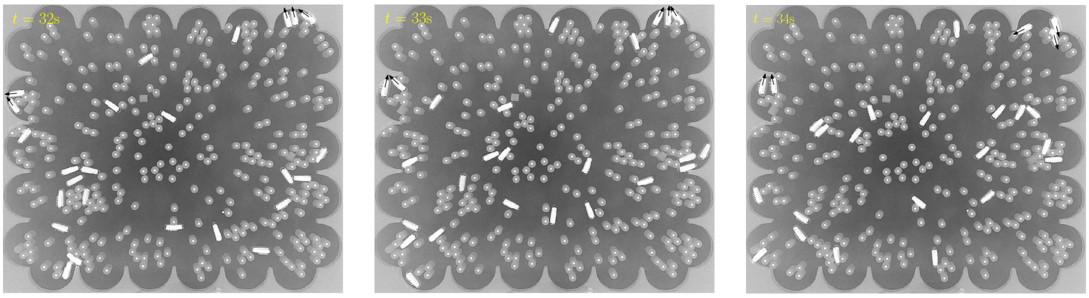

(a) $t = 32\,\text{s}$ **(b)** $t = 33\,\text{s}$ **(c)** $t = 34\,\text{s}$

Figure 3.9: An example showing congestion like behavior, in three consecutive frames, where the active particles hinder each other from moving when going in the opposite direction. Three particles in the upper right corner and two in the upper left corner, the particles being stuck are marked with black arrows showing their instantaneous orientation. The last frame at $t = 34\,\text{s}$ shows the three particles in the upper right corner just escaping out from the congestion while the two particles in the upper left corner are still being stuck.

This hindering behavior in fig. 3.9 happens more frequently as the number of active particles increases, and as a consequence, the ensemble mean velocity of the active particles decreases when this happens.
The differences that was seen when observing the active particles velocity as a function of number active particles is that, higher number of active particles leads to a velocity distribution peak at a lower velocity, and the explanation being, because of the stage being overpopulated with active particles, they hinder each other from moving as in fig. 3.9 which in turn leads to them having low velocity.
Regarding the number of obstacles, there is a strong intuition already about how this parameter should affect the active particles motion, after having seen the results before in fig. 3.7. The intuition is that the active particles velocity should decrease

as the number of obstacles increases. We confirm this by visualizing the probability density of the active particles velocity as a function of the number of obstacels in fig. 3.10.

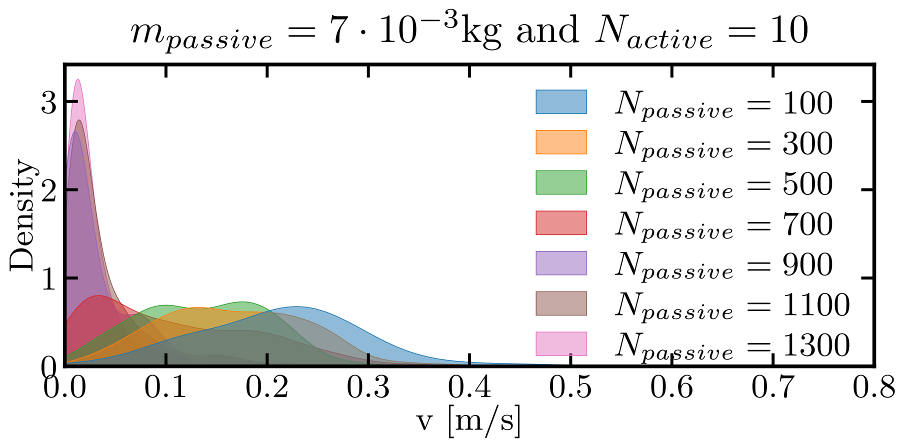

Figure 3.10: Active particles probability distribution as a function of obstacle density. The distribution shift to the left towards $v = 0$ as the the number of obstacles increases, an expected result since the active particles has less space to move on when the arena is filled with many obstacles.

Having shortly discussed before, the scenario where the obstacle weight do not have any significant effect on the active particles when the number of obstacles is low. The explanation was that when the obstacle density is too sparse, then the interaction between active particles and obstacles will be minimal, resulting in the different obstacle weight having no distinguishable effect on the active particles. Though intuition suggest that there certainly are differences between a bug colliding with a heavy object in oppose to a light object. Hitting a heavy object, the rod shaped bugs should "bounce" off changing its direction more rapidly than when hitting a light object.
To investigate this, the orientational changes of the bugs in terms angular velocity are being used, to see if their behaviors are expected and how do their orientation get affected by different parameters. The angular velocity is the change of orientation per time unit and can be expressed as

$$\omega = \frac{d\theta}{dt} \tag{3.3}$$

where ω is the angular velocity in unit $\mathrm{rad\,s^{-1}}$, θ is the orientation measured in rad. In fig. 3.11 shows how the obstacle weight affect the angular velocity of the active particles.
As can be observed in fig. 3.11, all of the cases has their peaks at $d\theta/dt \approx 0\,\mathrm{rad\,s^{-1}}$ while for $m_{\text{passive}} = 2 \times 10^{-3}\,\mathrm{kg}$(blue) the distribution peak is higher than for $m_{\text{passive}} = 17 \times 10^{-3}\,\mathrm{kg}$(red). This suggest that there is a higher probability for the active particles to change their orientation rapidly in an environment of heavy obstacles, more rapidly than with light obstacles. This points to what was mentioned earlier about

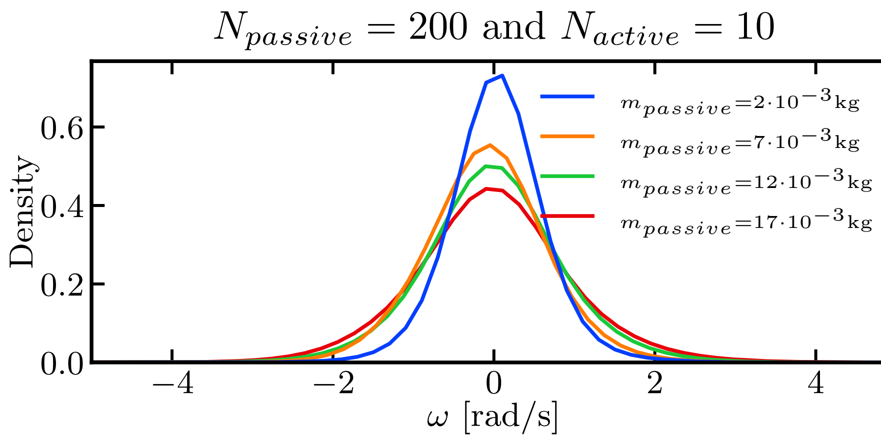

Figure 3.11: Distributions of the active particles angular velocity for different obstacle weights. The four distributions all peaks at $\omega \approx 0$, the distribution for lighter obstacle weight(blue) has a higher peak compared to the heavier one(red).

the nature of the collisions between active and passive particles. When the active particles collide with a heavy obstacle, the active particle will ”bounce off” and change their direction more abruptly, similar mechanics as in elastic collisions. In contrast with the scenario where the active particles collide with a light obstacle, they instead push the obstacle forward for a short distance, then slowly changing their direction before going on a new path.
Finally the angular velocity as a function of obstacle density and number of active particles is shown in fig. 3.12

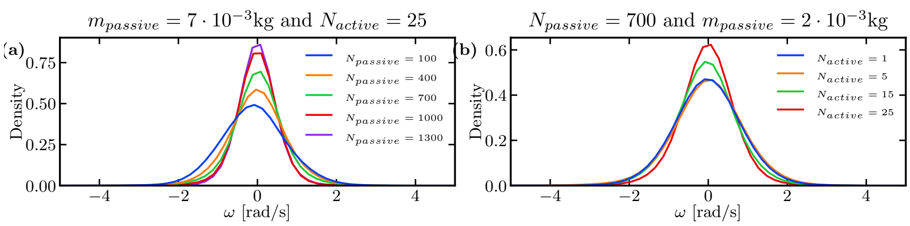

Figure 3.12: Varying obstacle density in **(a)** shows that the distribution peak is higher at $\omega \approx 0$ as the number of obstacles increases, compare 1300 obstacles(purple) and 100 obstacles(blue). In **(b)**, varying the number of active particles, shows a higher distibution peak at $\omega \approx 0$ for higher number of active particles(red), again a result of congestion.

Somewhat expected result in fig. 3.12, since it was already observed when studying the velocity where the velocity tend to be lower as the number of obstacles and the number of active particles increases. Similar pattern holds also for the angular velocity.

3.3 Collective Behaviours

One of the main focus of this thesis was to design a macroscale system in a way to provide the conditions for collective behaviors to emerge. To be more specific, we want to observe cooperative behaviors such as, active particles forming and reusing channels. Though this particular behavior is not the only cooperative behavior since any other behaviors/interactions between the active particles that are mutually beneficial can be classified as cooperative behavior. In our case, it is natural to define the goal for the active particles as maximizing their movements.
In the experiments, there were some frequently occurring behaviors with the bugs that was difficult to quantify. The easiest way was to do a qualitative observation by watching the recorded footage of the experiments. Some of these behaviors occurs more frequent than others and may seem trivial. In this section, different observed behaviors will be presented.
One behavior that happens in almost all the experiments is where the bugs become stuck at the boundary edges of the arena, see fig. 2.2. This was a big issue with the two previous designs of the border where we first had a rectangular border with 90° corners(right boundary in fig. 2.2 without the rounded corners) and the bugs kept getting stuck at these sharp corners. The second iteration had rounded corners which remove the issue of the first design but still have the problem of which the bugs would spend most of the time traversing the edges of the stage instead of interacting with the obstacles inside the stage. The current design which is the cloudy border would minimize these two previous problems, but the getting ”stuck” behavior still occur, but for different reasons. For the first two border designs, the bugs were getting stuck mainly because of the chirality of there movements in combination with the border design of straight edges with rounded or sharp corners. The chirality of these robots was a random property that could not be controlled in before hand, also given the fact that the robots are suppose to be toys for children, this unexpected property was no surprise.
With the current ”cloudy” border(left model in fig. 2.2) the bugs are instead getting stuck when they are going against each other in the opposite direction and they are in some sort of equilibrium where the forces from each bugs in different directions balance out and the group of bugs stay still for some seconds until the equilibrium breaks and each bugs go their own way again. Of course the chirality of the bugs and the stage design still plays a role in this but it is not obvious as in the previous two border designs. Moreover, the number of the bugs does play a role in this behavior where more number of bugs will make this congestion behavior happen more frequently, see for example the velocity distribution in fig. 3.8.
Some example of bugs getting stuck is shown in fig. 3.13.
The situation shown in fig. 3.13 is an example of the active particles working against each other by preventing each other from moving. This behavior can be categorised as ”Anti Cooperative Behaviour” i.e. some collective behavior that minimize the active particles movement, as oppose to Cooperative behavior where the bugs help each other to maximize the groups movements.
There are many scenarios where cooperative behavior occurs where the bugs assist each other to move in various ways, some easier to observed than others. Here some

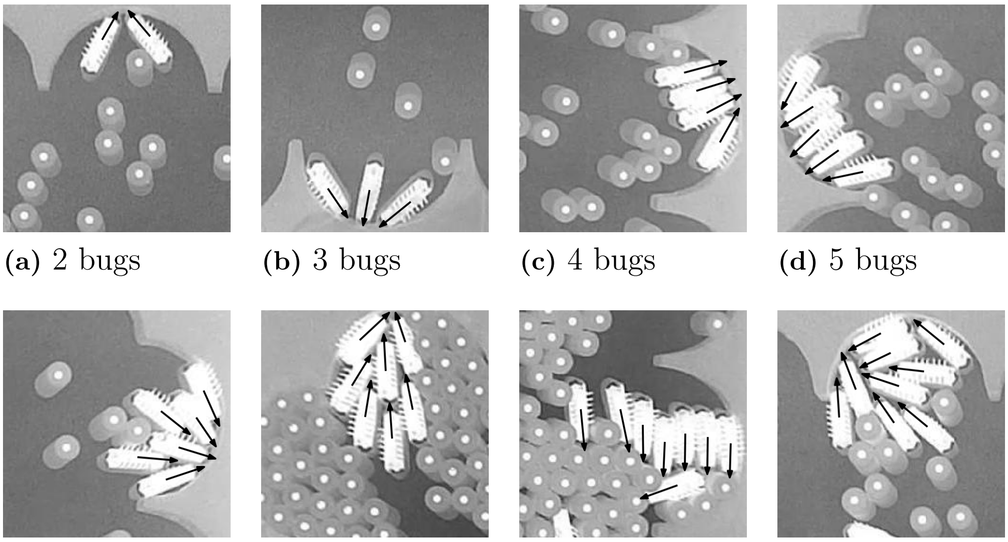

(a) 2 bugs **(b)** 3 bugs **(c)** 4 bugs **(d)** 5 bugs

(e) 6 bugs **(f)** 7 bugs **(g)** 8 bugs **(h)** 9 bugs

Figure 3.13: Example of situations where the bugs become stuck when coming in contact with one another and the border of the arena. The direction of where the bugs are pushing is marked with black arrows. Each figure shows different number of bugs that are involved, 2 bugs in **(a)**, 3 bugs in **(b)**, 4 bugs in **(c)**, 5 bugs in **(d)**, 6 bugs in **(e)**, 7 bugs in **(f)**, 8 bugs in **(g)** and 9 bugs in **(h)**

cases of cooperative behavior will be presented. With regard of the restrictions of this format, only the cases that can be clearly visualized will be presented. The first example is shown in fig. 3.14.

Here the bugs assist each other to push away some obstacles from the border of the arena, and thus making way for other bugs to move freely at the edges. The observation in fig. 3.14 is taken from three different experiments where in each experiment four consecutive frames are taken showing how the bugs move. Note that in these examples shown, the assistance of other bugs that were not initially pushing the obstacles do make a significant difference in moving them, either by speeding up the process or clearing out a bigger area of obstacles.

Next example is when the bugs are pushing onto each other preventing the scenario where some bugs are being blocked and confined by obstacles.

As for the case of cooperative behavior shown i fig. 3.15, where a push bug push another bug, the outcome where the pushing bug successfully push another bug from its unmovable position doesn't always happen. When the obstacle weight is too high and if there are too many obstacle in front of the bugs, both the bugs will become stuck. With that said, when two bugs do collide they tend to change each others movement in some way and thus destroy whatever equilibrium they were in, which will create more movements.

The motivation of categorising the above behaviors in figs. 3.14 and 3.15 as "Cooperative behaviors" can be put as follows. Since the aim of this project is to study the collective behaviors of these agents, and to do so, these agents have to "behave" in some way, and behaving in this particular case is almost synonymous with moving.

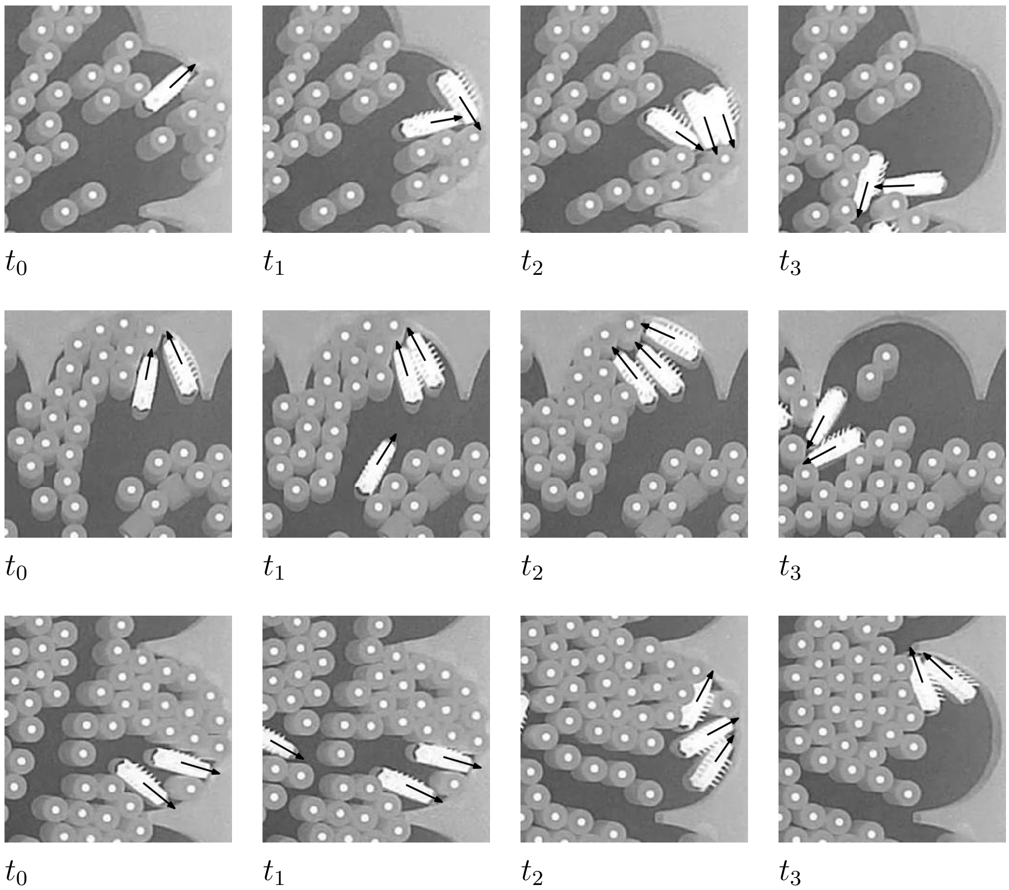

Figure 3.14: Three different examples of cooperative behavior showing how the bugs assist one another to push away obstacles. It would take much longer time without other bugs helping. The direction of the bugs is marked with black arrows.

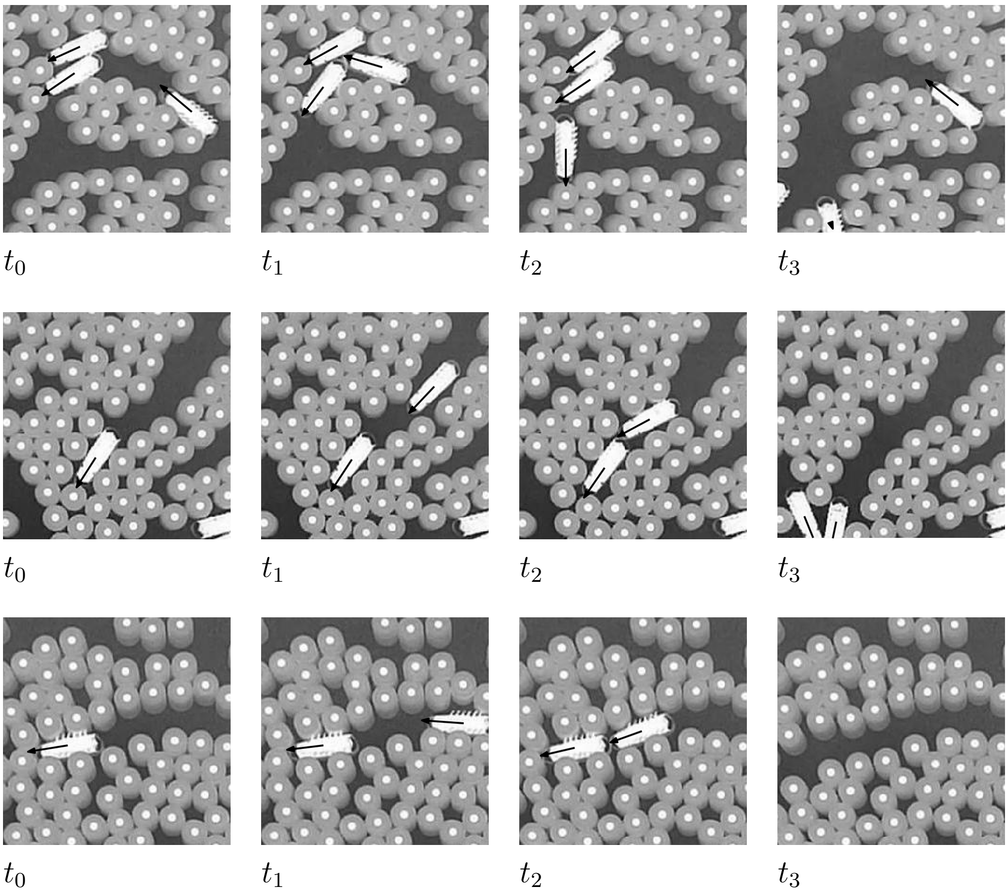

Figure 3.15: Examples of cooperative behavior where one bug push another bug that is being blocked, to move forward. When facing an obstacle one single bug might not be strong enough to move the obstacles in front, but when another bug join, they are able to together push the obstacle away making channels for other bugs.

Moving particles thus give interesting and non-trivial data for analysis, compared to a particle standing still from being blocked. So any action, from a particle onto another one, that increase the ensemble displacement will be considered as cooperative behavior.
Now the next reoccurring behavior, which is shown in fig. 3.16, is when the bugs create a circular shaped channel and keep reusing it, circling inside for many lapses.

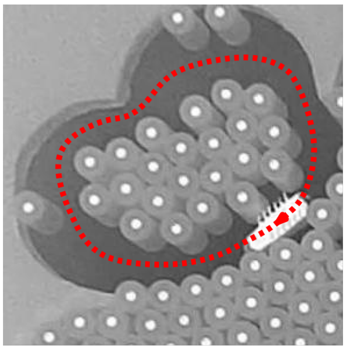

(a) 7 lapses

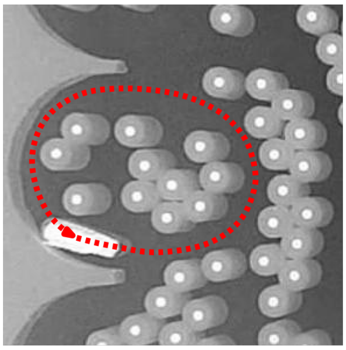

(b) 3 lapses

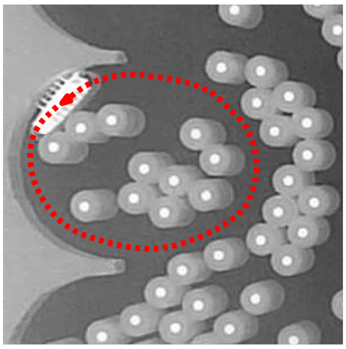

(c) 2 lapses

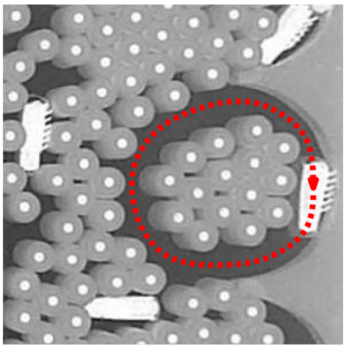

(d) 4 lapses

Figure 3.16: Examples where the bugs are circling inside a circle shaped channel for many lapses. The bugs might end up in this situation coming from other channels, and due to its chirality they might circle around for some lapse before moving on through nearby channels. In some cases while the bugs are circling, other bugs might push and move the obstacles adding walls to this circular shaped channels making them more stable. This leads to the bugs inside, the fully closed circular channel, traversing around for many lapses, as seen in **(a)** to **(d)**.

This circling behavior is presented in the four examples, figs. 3.16a to 3.16d, with the trajectories of the bugs marked in red and the number of lapses of which the bugs are circling around.
This type of ”local” channel i.e. not expanding over a large area of the arena, tend to be more stable than the channels that extend over a larger area. The reason for this is that for the latter type of channel, the likelihood of another bug cutting through and destroy the channel is higher. These circular shaped channels are mostly formed between rigid boundary from the stage(fig. 2.2) and obstacles, this means that a portion of the channel will be an immovable part supported by the

rigid bounday, and the movable part formed by the obstacles. This will decrease the chance of channels being destroyed since it is partly immovable.
Now the duration of the bugs circling in these channels will depend on how much of the channel consist of the rigid boundary, which is immovable by the bugs. In fig. 3.16a, the bug manage to stay in the channel for 7 lapses compared to the case in fig. 3.16c, which is only 2 lapses. One could immediately see the differences in these two channels where in the first case a big segment of the channel constitute of the rigid boundary made by wood, roughly two-thirds of the channel. Whereas the latter case where the bug only circle for 2 lapses, this channel constitute mostly of obstacles and empty spaces, roughly two-third of the channel being movable and one-third immovable, this will increase the likelihood of the bug destroying or escaping the channel.
Generally the channels tend to be quite unstable, especially the ones that cover a large area of the stage consisting only of obstacles and no rigid boundaries. Every time a bug uses a channel it moves the obstacles slightly, and after many usages, the channel is destroyed. A channel is destroyed faster when using light obstacles and high number of bugs.
An example of the type of channel that stretches across the stage is shown in fig. 3.17.

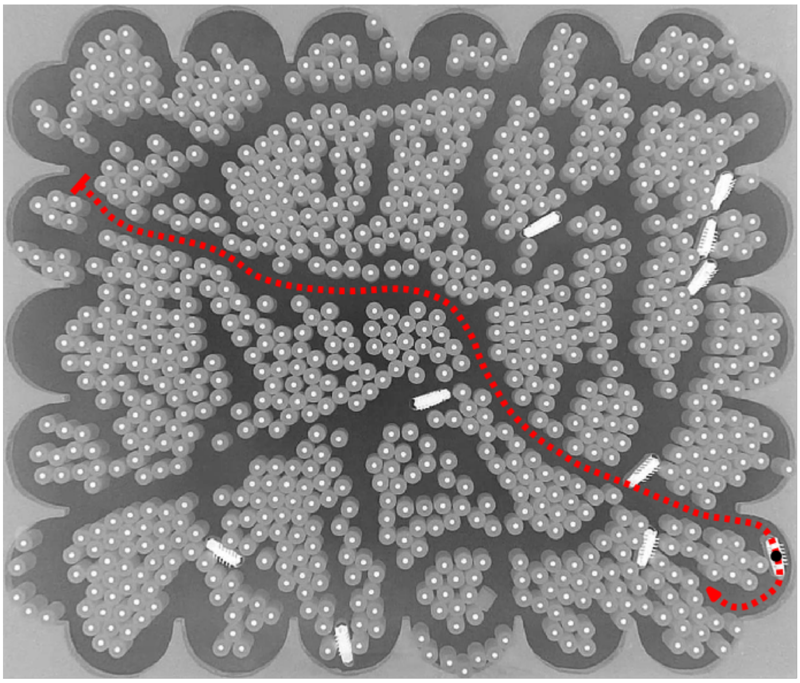

Figure 3.17: A bug propagating through a long channel that stretches over the stage, starting from the upper left corner going to the lower right corner. This experiment was done with $N_{\text{active}} = 10$, $N_{\text{passive}} = 900$ and $m_{\text{passive}} = 2 \times 10^{-3}$ kg. The trajectory of where the bug traverses along the channel is marked with a dashed red line, the start of the trajectory is marked as $\vdash$ and the end with $\rightarrow$. The bug that traverses this trajectory is marked with a black dot.

Again, these type of channel shown in fig. 3.17 tend to be unstable with reasons mentioned before. Compared to the circular shaped channels shown in fig. 3.16,

these long type are quite exposed to other bugs destroying it, by either pushing away the obstacles that make up the walls of the channels or moving some obstacles into the channel and thus blocking the channel.
With only 10 bugs in this experiment, in fig. 3.17, it is relatively easy to spot when a channel is being created, reuse and destroyed. When the number of bugs is higher than this, the stage gets somewhat cluttered which makes it harder to spot a channel and also the high number of bugs will raise the likelihood of a channel being destroyed.
With only one bug, it is easier to track its behavior, as seen in fig. 3.18.

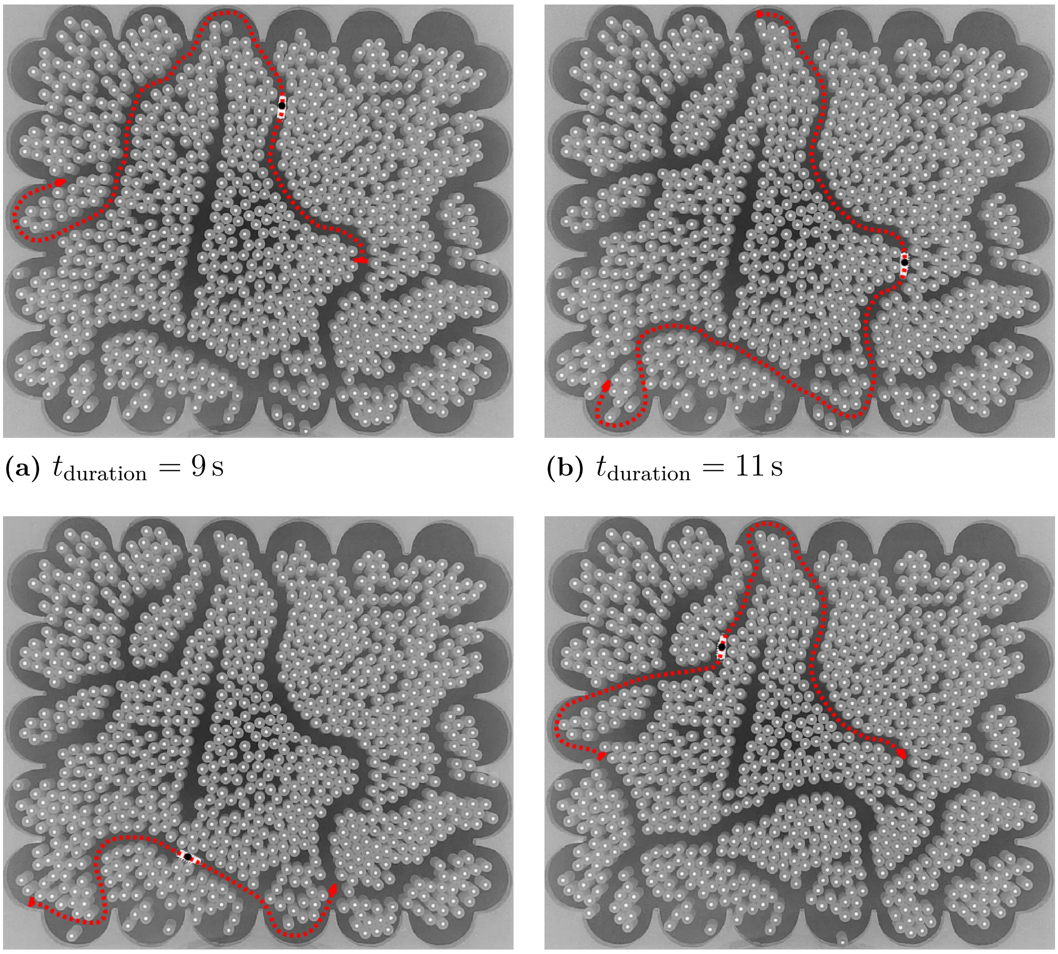

(a) $t_{\text{duration}} = 9\,\text{s}$ **(b)** $t_{\text{duration}} = 11\,\text{s}$

(c) $t_{\text{duration}} = 4\,\text{s}$ **(d)** $t_{\text{duration}} = 11\,\text{s}$

Figure 3.18: Four occurrences in the same experiment where a bug is reusing preexisting channels. Depending on the length of the channel, it takes different time for the bug to go through the whole channel ranging from $t_{\text{duration}} = 4\,\text{s}$ in **(c)** to $t_{\text{duration}} = 11\,\text{s}$ in **(b)** and **(d)**. Since there is only one bug in this experiment, this bug both create and reuse its own channel. This experiment was done with $N_{\text{active}} = 1$, $N_{\text{passive}} = 1000$ and $m_{\text{passive}} = 2 \times 10^{-3}\,\text{kg}$.

In this one bug case it is easy to spot the moment when the bug is using a channel, and some part of the channel last relatively long since there is no other bug that

can destroy the channel. The channels that are formed in the experiments with low number of bugs and high obstacle density tend to be longer in distance and more stable i.e. stay intact for a longer period of time. This can be visualized in figs. 3.18a to 3.18c, where the overall appearance of the stage, with the preexisting channels, looks close to identical. In the one bug example, in fig. 3.18 the duration for with the bug to reuse the different channels spans from $t_{\text{duration}} = 4\,\text{s}$ to $t_{\text{duration}} = 11\,\text{s}$, which are some of the longest duration observed amongst the different experiments regarding channel behaviors.
Another type of situation where several bugs reuse the same channel is presented in fig. 3.19.

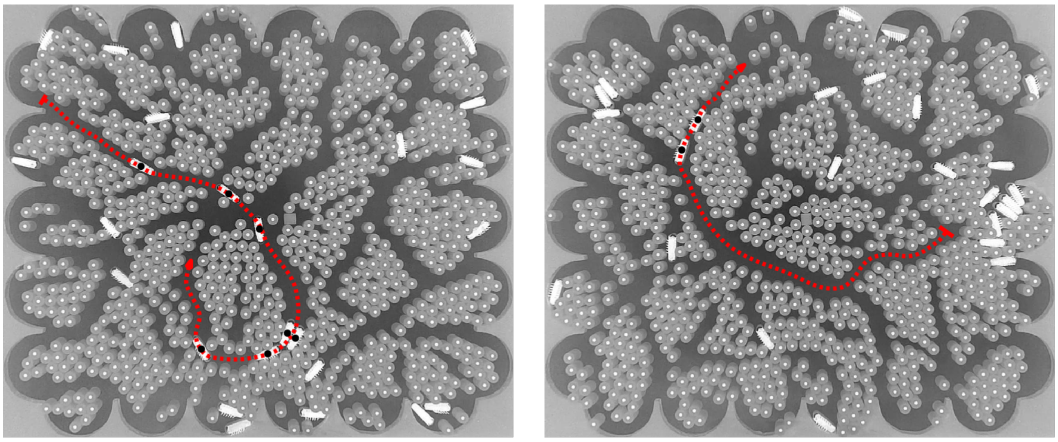

(a) (b)

Figure 3.19: Situation where several bugs traverse through the same channel, 7 bugs in **(a)** and 2 bugs in **(b)**. This experiment was done with $N_{\text{active}} = 25$, $N_{\text{passive}} = 900$ and $m_{\text{passive}} = 2 \times 10^{-3}\,\text{kg}$.

With the one bug example in fig. 3.18, its channelling behavior can also be observed by looking at the time evolution of its velocity v, reported in fig. 3.20.
This figure shows how the bugs velocity vary depending on its behavior, whether the bug is reusing an already existing channel or the bug is forming a new channel. When the bug is reusing a channel, its velocity oscillates around a relatively higher velocity(red segments in fig. 3.20) than when it is forming a channel(blue segments in fig. 3.20). This velocity differences is due to the simple fact that, when the bug is reusing a channel, it can move throgh obstacle-free spaces unhindered and is able to maintain its high speed throughout the stretch of the channel. On the other hand, when the bug is forming a channel, it instead spending most of it time pushing obstacles trying to form new channels, which will inevitably slow its speed down.

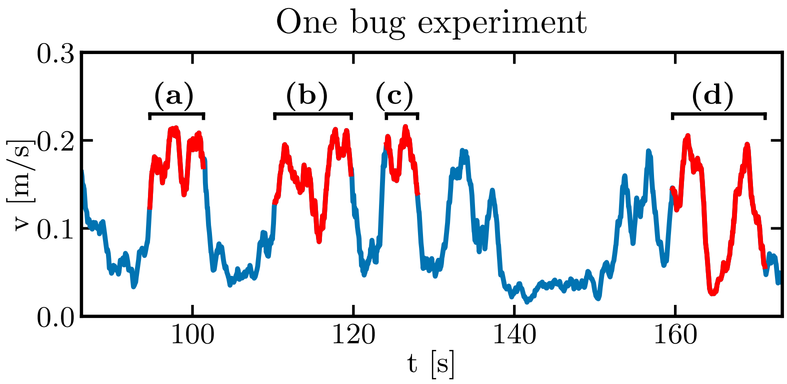

Figure 3.20: Velocity-time graph showing how the velocity of the bug in fig. 3.18, evolves through time. The red segments of the curve marked with **(a)**, **(b)**, **(c)** and **(d)** is the period when the bug is traversing through the channels shown in fig. 3.18. At the channel-using segments (red lines), the bugs velocity oscillate around a higher velocity than the blue segments, where the bug is instead forming channels. In the channel-using segment **(d)** there is a short velocity dip in the middle. Eventhough this being a channel-using segment, the bug collide against the walls of the channel and push for a short period of time before returning to going through the already existing channel again.

4
Conclusion

The field of active particles, though being a new field, is widely researched across multiple disciplines, such as statistical physics[43], biology[29], robotics[44], social transport[45], soft matter[46] and biomedicine[39].
While most of the researches in the the field of active particles are often done in the microscale with microorganisms[26]–[28]. There are yet grounds to be explored in the macroscale, which was the origin of this project.
What was seen here as the results of this project might strike to be somewhat intuitive and expected, with for example higher obstacle density or higher obstacle weight, leading to less motion for the active particles. Some results are less intuitive, such as higher number of active particles resulting in lower velocity for the active particles. However intuitive a result might be, it was interesting to go through the experiments to confirm the expectations.
Qualitative results was also presented as collective behaviors where we saw behaviors such as channel formation, reusing of channels, cooperative behaviors and other collective behaviors. These behaviors could only be observed clearly when the obstacle density was high.
Though it is obvious in hindsight that for example a bug will take a certain path or circling around one path or even pushing another bug because it has no where else to go, it is daunting that these behavior appears randomly when changing some parameters that do not have any obvious connection to these specific behaviors.
Emergent behaviors is one of key properties of complex systems. It is powerful to think that a system with simple agents can exhibit complex behaviors when some parameter is being tuned. This is the heart of our nature with simple cells that follows simple rules, but together can accomplish something as complex as the human body[58] or even the human brain[59]. Thought this field is still in its infancy, it is exciting to speculate what potential it has. The potential applications could be for examples drug delivery or elimination of cancer cells using nano robots. Fires could be put out by a swarm of drones, building could be built safer for evacuations using the knowledge of many particle systems simulation, or even designing autonomous robots for remote exploration such as rover in mars.
With all being presented here, there is still works to be done and it is encouraged for future works to improve what was done in this project, continuing to find better and smarter ways to study active-passive particles systems in macroscale. And hopefully this project contributes to advancing the field of active matter.

List of Figures

Bibliography

[1] Clemens Bechinger, Roberto Di Leonardo, Hartmut Löwen, et al. "Active particles in complex and crowded environments". In: *Reviews of Modern Physics* 88.4 (2016), p. 045006.

[2] Craig W Reynolds. *Flocks, herds and schools: A distributed behavioral model.* Vol. 21. 4. ACM, 1987.

[3] Tamás Vicsek, András Czirók, Eshel Ben-Jacob, et al. "Novel type of phase transition in a system of self-driven particles". In: *Physical review letters* 75.6 (1995), p. 1226.

[4] Hugues Chaté, Francesco Ginelli, Guillaume Grégoire, et al. "Modeling collective motion: variations on the Vicsek model". In: *The European Physical Journal B* 64.3 (2008), pp. 451–456.

[5] Robert Grossmann, Lutz Schimansky-Geier, and Pawel Romanczuk. "Self-propelled particles with selective attraction–repulsion interaction: from microscopic dynamics to coarse-grained theories". In: *New Journal of Physics* 15.8 (2013), p. 085014.

[6] Lucas Barberis and Fernando Peruani. "Large-scale patterns in a minimal cognitive flocking model: incidental leaders, nematic patterns, and aggregates". In: *Physical review letters* 117.24 (2016), p. 248001.

[7] Mite Mijalkov, Austin McDaniel, Jan Wehr, et al. "Engineering sensorial delay to control phototaxis and emergent collective behaviors". In: *Physical Review X* 6.1 (2016), p. 011008.

[8] Giovanni Volpe and Jan Wehr. "Effective drifts in dynamical systems with multiplicative noise: a review of recent progress". In: *Reports on Progress in Physics* 79.5 (2016), p. 053901.

[9] Kosuke Matsui and John J Molina. "Noise induced phase separation in active systems: Creating patterns with noise". In: *arXiv preprint arXiv:1702.02379* (2017).

[10] Dorilson S Cambui, M Godoy, and AS de Arruda. "Finite-size effects in simulations of self-propelled particles system". In: *Physica A: Statistical Mechanics and its Applications* 467 (2017), pp. 129–136.

[11] András Czirók, Eshel Ben-Jacob, Inon Cohen, et al. "Formation of complex bacterial colonies via self-generated vortices". In: *Physical Review E* 54.2 (1996), p. 1791.

[12] Jeremie Palacci, Stefano Sacanna, Asher Preska Steinberg, et al. "Living crystals of light-activated colloidal surfers". In: *Science* 339.6122 (2013), pp. 936–940.

[13] Isaac Theurkauff, Cécile Cottin-Bizonne, Jérémie Palacci, et al. "Dynamic clustering in active colloidal suspensions with chemical signaling". In: *Physical review letters* 108.26 (2012), p. 268303.

[14] Félix Ginot, Isaac Theurkauff, Demian Levis, et al. "Nonequilibrium equation of state in suspensions of active colloids". In: *Physical Review X* 5.1 (2015), p. 011004.

[15] Alexandre Morin, Nicolas Desreumaux, Jean-Baptiste Caussin, et al. "Distortion and destruction of colloidal flocks in disordered environments". In: *Nature Physics* 13.1 (2017), pp. 63–67.

[16] Jerome Buhl, David JT Sumpter, Iain D Couzin, et al. "From disorder to order in marching locusts". In: *Science* 312.5778 (2006), pp. 1402–1406.

[17] Pawel Romanczuk, Markus Bär, Werner Ebeling, et al. "Active brownian particles". In: *The European Physical Journal Special Topics* 202.1 (2012), pp. 1–162.

[18] Peter Reimann. "Brownian motors: noisy transport far from equilibrium". In: *Physics reports* 361.2-4 (2002), pp. 57–265.

[19] Benjamin M Friedrich and Frank Jülicher. "Chemotaxis of sperm cells". In: *Proceedings of the National Academy of Sciences* 104.33 (2007), pp. 13256–13261.

[20] Dávid Selmeczi, Liwen Li, Lykke II Pedersen, et al. "Cell motility as random motion: A review". In: *The European Physical Journal Special Topics* 157.1 (2008), pp. 1–15.

[21] Hendrik Ulrich Boedeker, Carsten Beta, Till D Frank, et al. "Quantitative analysis of random ameboid motion". In: *EPL (Europhysics Letters)* 90.2 (2010), p. 28005.

[22] PM Kareiva and N Shigesada. "Analyzing insect movement as a correlated random walk". In: *Oecologia* 56.2-3 (1983), pp. 234–238.

[23] Niko Komin, Udo Erdmann, and Lutz Schimansky-Geier. "Random walk theory applied to Daphnia motion". In: *Fluctuation and Noise letters* 4.01 (2004), pp. L151–L159.

[24] Walter F Paxton, Kevin C Kistler, Christine C Olmeda, et al. "Catalytic nanomotors: autonomous movement of striped nanorods". In: *Journal of the American Chemical Society* 126.41 (2004), pp. 13424–13431.

[25] Jonathan R Howse, Richard AL Jones, Anthony J Ryan, et al. "Self-motile colloidal particles: from directed propulsion to random walk". In: *Physical review letters* 99.4 (2007), p. 048102.

[26] Eric Lauga and Thomas R Powers. "The hydrodynamics of swimming microorganisms". In: *Reports on Progress in Physics* 72.9 (2009), p. 096601.

[27] Michael E Cates. "Diffusive transport without detailed balance in motile bacteria: does microbiology need statistical physics?" In: *Reports on Progress in Physics* 75.4 (2012), p. 042601.

[28] WCK Poon. "From Clarkia to Escherichia and Janus: The physics of natural and synthetic active colloids". In: *Proc. Int. Sch. Phys. Enrico Fermi* 184 (2013), pp. 317–386.

[29] Gandhimohan M Viswanathan, Marcos GE Da Luz, Ernesto P Raposo, et al. *The physics of foraging: an introduction to random searches and biological encounters*. Cambridge University Press, 2011.

[30] Dušan Babič, Carmen Schmitt, and Clemens Bechinger. “Colloids as model systems for problems in statistical physics”. In: *Chaos: An Interdisciplinary Journal of Nonlinear Science* 15.2 (2005), p. 026114.

[31] Frank Schweitzer, Werner Ebeling, and Benno Tilch. “Complex motion of Brownian particles with energy depots”. In: *Physical Review Letters* 80.23 (1998), p. 5044.

[32] Werner Ebeling, Frank Schweitzer, and Benno Tilch. “Active Brownian particles with energy depots modeling animal mobility”. In: *BioSystems* 49.1 (1999), pp. 17–29.

[33] Udo Erdmann and Werner Ebeling. “Collective motion of Brownian particles with hydrodynamic interactions”. In: *Fluctuation and Noise Letters* 3.02 (2003), pp. L145–L154.

[34] Frank Schweitzer. *Brownian agents and active particles: collective dynamics in the natural and social sciences*. Springer Science & Business Media, 2003.

[35] P Romanczuk, U Erdmann, H Engel, et al. “Beyond the keller-segel model”. In: *The European Physical Journal Special Topics* 157.1 (2008), pp. 61–77.

[36] Stephen J Ebbens and Jonathan R Howse. “In pursuit of propulsion at the nanoscale”. In: *Soft Matter* 6.4 (2010), pp. 726–738.

[37] Giorgio Volpe, Sylvain Gigan, and Giovanni Volpe. “Simulation of the active Brownian motion of a microswimmer”. In: *American Journal of Physics* 82.7 (2014), pp. 659–664.

[38] Bradley J Nelson, Ioannis K Kaliakatsos, and Jake J Abbott. “Microrobots for minimally invasive medicine”. In: *Annual review of biomedical engineering* 12 (2010), pp. 55–85.

[39] Joseph Wang and Wei Gao. “Nano/microscale motors: biomedical opportunities and challenges”. In: *ACS nano* 6.7 (2012), pp. 5745–5751.

[40] Debabrata Patra, Samudra Sengupta, Wentao Duan, et al. “Intelligent, self-powered, drug delivery systems”. In: *Nanoscale* 5.4 (2013), pp. 1273–1283.

[41] Loai KEA Abdelmohsen, Fei Peng, Yingfeng Tu, et al. “Micro-and nanomotors for biomedical applications”. In: *Journal of Materials Chemistry B* 2.17 (2014), pp. 2395–2408.

[42] Wei Gao and Joseph Wang. “The environmental impact of micro/nanomachines: a review”. In: *Acs Nano* 8.4 (2014), pp. 3170–3180.

[43] Sriram Ramaswamy. “The mechanics and statistics of active matter”. In: (2010).

[44] Manuele Brambilla, Eliseo Ferrante, Mauro Birattari, et al. “Swarm robotics: a review from the swarm engineering perspective”. In: *Swarm Intelligence* 7.1 (2013), pp. 1–41.

[45] Dirk Helbing. “Traffic and related self-driven many-particle systems”. In: *Reviews of modern physics* 73.4 (2001), p. 1067.

[46] M Cristina Marchetti, Jean-François Joanny, Sriram Ramaswamy, et al. “Hydrodynamics of soft active matter”. In: *Reviews of Modern Physics* 85.3 (2013), p. 1143.

[47] Simon Nilsson and Giovanni Volpe. “Metastable clusters and channels formed by active particles with aligning interactions”. In: *New Journal of Physics* 19.11 (2017), p. 115008.

[48] John Toner, Yuhai Tu, and Sriram Ramaswamy. “Hydrodynamics and phases of flocks”. In: *Annals of Physics* 318.1 (2005), pp. 170–244.

[49] Yue-Xian Li, Ryan Lukeman, and Leah Edelstein-Keshet. “Minimal mechanisms for school formation in self-propelled particles”. In: *Physica D: Nonlinear Phenomena* 237.5 (2008), pp. 699–720.

[50] Eric Bertin, Michel Droz, and Guillaume Grégoire. “Hydrodynamic equations for self-propelled particles: microscopic derivation and stability analysis”. In: *Journal of Physics A: Mathematical and Theoretical* 42.44 (2009), p. 445001.

[51] Howard C Berg. *E. coli in Motion*. Springer Science & Business Media, 2008.

[52] Roseanne M Ford and Ronald W Harvey. “Role of chemotaxis in the transport of bacteria through saturated porous media”. In: *Advances in Water Resources* 30.6-7 (2007), pp. 1608–1617.

[53] *HEXBUG nano® (random color)*. URL: `https://www.hexbug.com/hexbug-nano-single.html#description`.

[54] *Christmas Festical Trick Toy Solar Energy Moving Bug - Buy Solar Energy Moving Bug,Christmas Trick Toy,Solar Toy Product on Alibaba.com*. URL: `https://www.alibaba.com/product-detail/Christmas-Festical-Trick-Toy-Solar-Energy_60167590085.html?spm=a2700.details.deiletai6.1.77d5104dMQu7Bq`.

[55] Fernando Peruani. “From individual to collective motion of self-propelled particles: The role of particle shape, orientational ordering and clustering”. In: (2008).

[56] *AC200*. URL: `https://www.govicture.com/ac200`.

[57] URL: `https://www.amazon.co.uk/Victure-Actioncam-Waterproof-Underwater-Accessories-1080P/dp/B06XKZ6VH4`.

[58] Cindy E Hmelo-Silver and Roger Azevedo. “Understanding complex systems: Some core challenges”. In: *The Journal of the learning sciences* 15.1 (2006), pp. 53–61.

[59] David Meunier, Renaud Lambiotte, Alex Fornito, et al. “Hierarchical modularity in human brain functional networks”. In: *Frontiers in neuroinformatics* 3 (2009), p. 37.